



Predictions for Bottomonium from a Relativistic Screened Potential Model

Chaitanya Anil Bokade[†]  Bhaghyesh[‡] 

Department of Physics, Manipal Institute of Technology Manipal Academy of Higher Education, Manipal, 576104, Karnataka, India

Abstract: In this work, a comprehensive analysis of the mass spectra and decay properties of bottomonium states using a relativistic screened potential model is carried out. The mass spectrum, decay constants, $E1$ transitions, $M1$ transitions, and annihilation decay widths are evaluated. The interpretation of $\Upsilon(10355)$, $\Upsilon(10580)$, $\Upsilon(10860)$, and $\Upsilon(11020)$ as $S-D$ mixed bottomonium states are analysed. The $\Upsilon(10355)$ state is considered to be $3S-2D$, $\Upsilon(10580)$ and $\Upsilon(10753)$ are considered to be $4S-3D$ mixed states, and the $\Upsilon(10860)$ and $\Upsilon(11020)$ are deemed to be $5S-4D$ mixed states.

Keywords: Bottomonium, Relativistic Potential Model, Screened Potential, Radiative Decays, $S-D$ Mixing

DOI: **CSTR:**

I. INTRODUCTION

The study of heavy quarkonium, specifically bottomonium, has emerged as a captivating and influential field in contemporary particle physics. The allure of this research lies not only in the experimental endeavors aimed at unraveling the intricate properties of these heavy quark systems [1, 2], but also its rich theoretical framework which allows to understand intricate interplay of perturbative and non-perturbative quantum chromodynamics (QCD) phenomena across a broad energy spectrum [3]. The history of bottomonium traces back to $\Upsilon(1S)$, first discovered by the E288 Collaboration at Fermilab along with $\Upsilon(2S)$ and $\Upsilon(3S)$ [4, 5]. In 1982, the $\chi_{bj}(2P)$ states were observed from CUSB detector at CESR in $\Upsilon(3S) \rightarrow \gamma\chi_{bj}(2P)$ for $(J=0,1,2)$ [6, 7]. The $\chi_{bj}(1P)$ states were discovered in 1983 in $\eta_b(2S) \rightarrow \gamma\chi_{bj}(1P)$ and $\chi_{bj}(1P) \rightarrow \gamma\eta_b(1S)$ [8], and were later confirmed in the same year by CESR in $\Upsilon(2S) \rightarrow \gamma\chi_{bj}(1P) \rightarrow \gamma\Upsilon(1S)$ [9]. In 2005, most precise measurement of branching fractions and photon energies of $\chi_{bj}(1P)$ and $\chi_{bj}(2P)$ were conducted by the CLEO Collaboration [10]. For the first time in 1980, CESR observed a peak above the $B\bar{B}$ threshold and suggested it as $\Upsilon(4S)$ [11]. Later in 1985, CLEO at CESR, in addition to $\Upsilon(4S)$, reported the observation of $\Upsilon(10860)$ and $\Upsilon(11020)$ resonances [12]. Most recently, Belle Collaboration in 2019 measured $e^+e^- \rightarrow \Upsilon(1,2,3S)\pi^+\pi^-$ cross sections, determining masses and widths of $\Upsilon(10860)$ and

$\Upsilon(11020)$ with improved precision [13]. In 2004, CLEO Collaboration observed the $\Upsilon(1D)$ state at $10161.1 \pm 0.6 \pm 1.6$ MeV via a photon cascade of $\Upsilon(3S)$ decays, identifying it as $\Upsilon_2(1D)$ state [14]. BABAR Collaboration later confirmed the $\Upsilon_J(1D)$ triplet in $\Upsilon(3S) \rightarrow \gamma\Upsilon(1D) \rightarrow \gamma\pi^+\pi^-\Upsilon(1S)$, with significance of 5.8σ for $\Upsilon_2(1D)$, while the significance for $\Upsilon_1(1D)$ and $\Upsilon_3(1D)$ states were very low [15]. In 2008, BABAR discovered $\eta_b(1S)$ with 10σ significance via $\Upsilon(3S) \rightarrow \gamma\eta_b(1S)$ [16]. It was later confirmed by CLEO Collaboration [17, 18], which also identified $\eta_b(2S)$ with 5σ significance in $\Upsilon(2S) \rightarrow \gamma\eta_b(2S)$ [18]. Belle Collaboration observed $\eta_b(2S)$ for the first time in $h_b(2P) \rightarrow \gamma\eta_b(2S)$, measuring its mass as $9999.0 \pm 3.5^{+2.8}_{-1.9}$ MeV and hyperfine splitting as $m[\Upsilon(2S)] - m[\eta_b(2S)] = 24.3^{+4.0}_{-4.5}$ MeV [19]. In 2011, BABAR Collaboration observed $h_b(1P)$ with 3.1σ significance in $\Upsilon(3S) \rightarrow \pi^0 h_b(1P) \rightarrow \pi^0 \gamma \eta_b(1S)$ [20]. Belle Collaboration later confirmed $h_b(1P)$ in $\Upsilon(5S) \rightarrow \pi^+\pi^- h_b(1P)$ and discovered $h_b(2P)$ with 11.2σ significance, having mass of $10259.8 \pm 0.6^{+1.4}_{-1.0}$ MeV [21]. In 2012, ATLAS Collaboration observed $\chi_b(3P)$ in $\chi_b(nP) \rightarrow \gamma\Upsilon(1S,2S)$ [22], later it was also confirmed by D0 Collaboration with 5.6σ significance at mass barycentre of $10551 \pm 14 \pm 17$ MeV [23]. In 2018, CMS Collaboration observed $\chi_{b1}(3P)$ and $\chi_{b2}(3P)$ in $\gamma\Upsilon(3S)$ decay mode, measuring their masses as $10513.42 \pm 0.41 \pm 0.18$ MeV and $10524.02 \pm 0.57 \pm 0.17$ MeV, respectively, and a mass difference of $10.60 \pm 0.64 \pm 0.17$ MeV [24]. In 2012, from

Received 7 January 2025; Accepted 10 March 2025

[†] E-mail: anshul497@gmail.com

[‡] E-mail: bhaghyesh.mit@manipal.edu



Content from this work may be used under the terms of the Creative Commons Attribution 3.0 licence. Any further distribution of this work must maintain attribution to the author(s) and the title of the work, journal citation and DOI. Article funded by SCOAP³ and published under licence by Chinese Physical Society and the Institute of High Energy Physics of the Chinese Academy of Sciences and the Institute of Modern Physics of the Chinese Academy of Sciences and IOP Publishing Ltd

the data on $\Upsilon(5S)$ decays to $\Upsilon(nS)\pi^+\pi^-$ ($n = 1, 2, 3$) and $h_b(mP)\pi^+\pi^-$ ($m = 1, 2$), Belle Collaboration observed two charged structures, $Z_b(10610)$ and $Z_b(10650)$ [25]. Due to their charged property, they cannot be described in conventional quarkonium picture and require a four-quark configuration description such as hadronic molecules [26, 27], tetraquarks [28, 29], etc. In 2019, BELLE Collaboration discovered $\Upsilon(10753)$ with 5.2σ significance in $e^+e^- \rightarrow \Upsilon(nS)\pi^+\pi^-$ with mass of $10752.7 \pm 5.9_{-1.1}^{+0.7}$ MeV and width of $35.5_{-11.3-3.3}^{+17.6+3.9}$ MeV [30]. It was also identified through cross-section calculations by BABAR and BELLE experiments [31]. Even with significant progress in experimental domain there is still lack of key details, such as the total width and mass values of higher resonance, branching ratios for significant decay modes, etc. Unlike the rich charmonium-like XYZ sector, there are only few unconventional bottomonium-like states (e.g. $Z_b(10610)$, $Z_b(10650)$) that has been discovered. No experimental evidence exists for X_b , the bottomonium counterpart of $X(3872)$ [32]. The pursuit of similar exotic states in the bottomonium system, such as the X_b whose existence is predicted in multiple models [33, 34], holds promise for understanding the nature of the internal structure of $X(3872)$. Exotic hadron studies have predominantly relied on e^+e^- annihilation experiments, exemplified by BESIII, Belle, BaBar, and CLEO [3]. Belle II at SuperKEKB aims to achieve for a peak luminosity of $8 \times 10^{35} \text{cm}^2 \text{s}^{-1}$ by 2025, with operations extending to 2027 to collect over 50ab^{-1} of data [3]. Following the LHCb Upgrade I, Run-3 data will be crucial, while the PANDA experiment on antiproton-nucleon interactions and upcoming super τ - charm factories offer promising avenues for exploring novel states [2, 35]. In view of the potential for discovering new states in the bottomonium sector, we have developed a relativistic screened potential model that has proven effective for charmonium [36]. The proposed model provides a robust theoretical framework by considering relativistic effects and the screening of the potential. Our model can facilitate the identification and characterization of new and exotic states within the bottomonium spectrum.

In this paper we have conducted a comprehensive study of bottomonium in a relativistic screened potential model. In section II, we discuss the theoretical model used to describe the bottomonium bound system and the numerical approach used to solve the relativistic Schrodinger equation. Decay constants and various decays are discussed in section III. In section IV, $S - D$ mixing of bottomonium states is discussed. In section V a thorough investigation of our evaluation and interpretation of bottomonium states are conducted, along with comparison between the experimental results and other theoretical models. In section VI we present our conclusion.

II. METHODOLOGY

A relativistic potential model is developed to investigate various bottomonium properties. We utilize the spinless Salpeter equation, which is a relativistic extension of the Schrodinger equation [37]

$$H = \sqrt{-\nabla_q^2 + m_q^2} + \sqrt{-\nabla_{\bar{q}}^2 + m_{\bar{q}}^2} + V(r), \quad (1)$$

where $\vec{r} = \vec{x}_{\bar{q}} - \vec{x}_q$, $\vec{x}_{\bar{q}}$ and \vec{x}_q are the coordinates of the quarks and operators ∇_q^2 and $\nabla_{\bar{q}}^2$ are the partial derivatives of those coordinates respectively. m_q and $m_{\bar{q}}$ are the masses of quark and an anti-quark respectively. The interaction potential $V(r)$ between the quark and antiquark is composed of two components: $V_V(r)$, representing the one-gluon-exchange coulomb potential term that is dominant at short distance, and $V_S(r)$, which represents the linear confining term adjusted to account for colour screening effects at longer distances [38]:

$$V_V(r) = -\frac{4}{3} \frac{\alpha_s(r)}{r}, \quad (2)$$

$$V_S(r) = \lambda \left(\frac{1 - e^{-\mu r}}{\mu} \right) + V_0, \quad (3)$$

$$V(r) = V_V(r) + V_S(r). \quad (4)$$

Here λ is the linear potential slope and μ is the screening factor which regulates the behaviour of the long-range component of $V(r)$, causing it to flatten out as r becomes much larger than $1/\mu$ and exhibit a linear increase as r becomes much smaller than $1/\mu$. The $V(r)$ converges to Cornell potential as $\mu \rightarrow 0$ [38]. $\alpha_s(r)$ is the running coupling constant in coordinate space obtained by Fourier transformation of coupling constant in momentum space $\alpha_s(Q^2)$ [37] and is given by

$$\alpha_s(r) = \sum_i \alpha_i \frac{2}{\sqrt{\pi}} \int_0^{\gamma_i r} e^{-x^2} dx, \quad (5)$$

where α_i 's are the free parameters to imitate the short-distance behaviour of $\alpha_s(Q^2)$ as predicted by QCD. The parameters values are taken as $\alpha_1 = 0.15$, $\alpha_2 = 0.15$, $\alpha_3 = 0.20$, and $\gamma_1 = 1/2$, $\gamma_2 = \sqrt{10}/2$, $\gamma_3 = \sqrt{1000}/2$ [39]. The Hamiltonian H is solved as an eigenvalue equation using the method developed in [39, 40]. The Hamiltonian Eq. (1) as a eigen equation is given by

$$E\Psi(\vec{r}) = \left[\sqrt{-\nabla_q^2 + m_q^2} + \sqrt{-\nabla_{\bar{q}}^2 + m_{\bar{q}}^2} + V(r) \right] \Psi(\vec{r}). \quad (6)$$

The wave function can be expanded using spectral in-

tegration, which allows us to express the wave function as an integral over the eigenstates of the Hamiltonian H :

$$\Psi(\vec{r}) = \int d^3 r' \int \frac{d^3 k}{(2\pi)^3} e^{i\vec{k}(\vec{r}-\vec{r}')} \Psi(\vec{r}'). \quad (7)$$

Eq. (1) can be rewritten as

$$E\Psi(\vec{r}) = \int d^3 r' \frac{d^3 k}{(2\pi)^3} \left(\sqrt{k^2 + m_q} + \sqrt{k^2 + m_{\bar{q}}} \right) e^{i\vec{k}(\vec{r}-\vec{r}')} \Psi(\vec{r}') + V(r)\Psi(\vec{r}). \quad (8)$$

The exponential term can be expanded in terms of spherical harmonics as

$$e^{i\vec{k}\cdot\vec{r}} = 4\pi \sum_{nl} Y_{nl}^*(\hat{k}) Y_{nl}(\hat{r}) j_l(kr) i^l, \quad (9)$$

where j_l is the spherical Bessel function, $Y_{nl}(\hat{k})$ and $Y_{nl}(\hat{r})$ are the spherical harmonics with normalization condition $\int d\Omega Y_{n_1 l_1}(\hat{k}) Y_{n_2 l_2}(\hat{r}) = \delta_{n_1 n_2} \delta_{l_1 l_2}$, \hat{k} and \hat{r} are unit vectors along the \vec{k} and \vec{r} direction, respectively. The wave function can be factorized into radial $R_l(r)$ and angular $Y_{nl}(r)$ parts, and substituting Eq. (9) in (8) and simplifying, we get [39, 40]

$$Eu_l(r) = \frac{2}{\pi} \int dk k^2 \int dr' r' \left(\sqrt{k^2 + m_q^2} + \sqrt{k^2 + m_{\bar{q}}^2} \right) \times j_l(kr) j_l(kr') u_l(r') + V(r) u_l(r), \quad (10)$$

where $u_l(r)$ is the reduced radial wave function ($R_l(r) = u_l(r)/r$). When the separation distance grows for a quark-antiquark bound state, the wavefunction gradually decreases and eventually approaches zero at sufficiently large distance. In order to represent this behaviour, a characteristic distance scale L is introduced, confining the bound state's wavefunction within the spatial interval of $0 < r < L$. Next, one can expand the reduced wavefunction $u_l(r)$ in terms of spherical Bessel function for angular momentum l as

$$u_l(r) = \sum_{n=1}^{\infty} c_n \frac{a_n r}{L} j_l\left(\frac{a_n r}{L}\right), \quad (11)$$

where c_n 's are the expansion coefficients, a_n are the n -th root of the spherical Bessel function, $j_l(a_n) = 0$. For large value of N Eq. (11) can be truncated. The momentum is discretized as a result of confinement of space, which allows us to replace $a_n/L \leftrightarrow k$ and the integration in Eq. (10) can be replaced by $\int dk \rightarrow \sum_n \Delta a_n/L$, where, $\Delta a_n = a_n - a_{n-1}$. For finite space interval, $0 < r, r' < L$, incorporating all the changes in the Eq. (10), we get the fi-

nal equation in terms of the coefficients c_n 's as [39, 40]

$$Ec_m = \sum_{n=1}^N \frac{a_n}{N_m^2 a_m} \int_0^L dr V(r) r^2 j_l\left(\frac{a_n r}{L}\right) \left(\frac{a_n r}{L}\right) c_n + \frac{2}{\pi L^3} \left[\sqrt{\left(\frac{a_m}{L}\right)^2 + m_q^2} + \sqrt{\left(\frac{a_m}{L}\right)^2 + m_{\bar{q}}^2} \right] \Delta a_m a_m^2 N_m^2 c_m. \quad (12)$$

where N_m is module of spherical Bessel function

$$N_m^2 = \int_0^L dr' r'^2 j_l\left(\frac{a_m r'}{L}\right)^2. \quad (13)$$

When L and N attain sufficiently large values, the solution tends to become nearly stationary [39, 40]. The spin dependent interaction potential is given by [41, 42]

$$V_{SD}(r) = V_{SS}(r) \vec{S}_q \cdot \vec{S}_{\bar{q}} + V_{LS}(r) \vec{L} \cdot \vec{S} + V_T(r) S_{12}. \quad (14)$$

V_{SS} is the spin singlet-triplet hyperfine splitting term given by

$$V_{SS}(r) = \frac{32\pi\alpha_s(r)}{9m_q^2} \tilde{\delta}_\sigma(r). \quad (15)$$

Here $\tilde{\delta}_\sigma(r) = \left(\frac{\sigma}{\sqrt{\pi}}\right)^3 e^{-\sigma^2 r^2}$ is the smeared delta function [43, 44]. To regularize the non-zero hyperfine splitting, smearing of delta function as Gaussian of width $1/\sigma$ is necessary [43, 44]. The spin orbit term V_{LS} and the tensor term V_T which describe the fine structure splitting of the states are given by

$$V_{LS}(r) = \frac{1}{2m_q^2 r} (3V'_V(r) - V'_S(r)), \quad (16)$$

$$V_T(r) = \frac{1}{m_q^2} \left(\frac{V'_V(r)}{r} - V''_V(r) \right).$$

The tensor operator $S_{12} = 3(\vec{S}_q \cdot \hat{r})(\vec{S}_{\bar{q}} \cdot \hat{r}) - \vec{S}_q \cdot \vec{S}_{\bar{q}}$, has non-vanishing diagonal matrix elements only between $L > 0$ spin-triplet states. The spin-dependent interactions are diagonal in a $|J, L, S\rangle$ basis with matrix elements given by [43–45]

$$\langle \vec{S}_q \cdot \vec{S}_{\bar{q}} \rangle = \frac{1}{2} S^2 - \frac{3}{4},$$

$$\langle \vec{L} \cdot \vec{S} \rangle = \frac{1}{2} [J(J+1) - L(L+1) - S(S+1)],$$

$$\langle S_{12} \rangle = \begin{cases} -\frac{L}{6(2L+3)} & J = L+1 \\ \frac{1}{6} & J = L \\ -\frac{L+1}{6(2L-1)} & J = L-1. \end{cases} \quad (17)$$

Eq. (12) represents an eigenvalue equation in matrix form, which is solved numerically. The eigenvalues correspond to the masses of spin-averaged states and the eigenvectors represent their wave functions. Using the obtained normalized wave functions for the spin-averaged states, the spin-dependent corrections are evaluated perturbatively. The model parameters are determined using the χ^2 fit method through minimizing the χ^2 , defined as

$$\chi^2 = \sum_i \left(\frac{M_{Exp}^i - M_{Th}^i}{M_{Er}^i} \right)^2, \quad (18)$$

where M_{Exp}^i and M_{Th}^i are the experimental mass and predicted mass respectively, and M_{Er}^i is the error in M_{Exp}^i . The errors of observed masses M_{Er}^i are taken as 0.1% of the masses of the respective states, M_{Exp}^i . These errors are different from their corresponding experimental uncertainties, which are too small for some states and are unevenly distributed. This approach ensures balanced weighting in the fitting process and prevents states which have lower experimental errors from disproportionately influencing the fit [46]. For fitting we have considered the well established four S -wave states $\eta_b(1S, 2S)$, $\Upsilon(1S, 2S)$, four P -wave states $h_c(1P, 2P), \chi_{b1}(1P, 2P)$ and one D -wave state, 1^3D_2 . Using this approach, we obtain a χ^2 value of 14.1. The fitted parameters are listed in Table 1. The masses of S, P, D, F and G states are presented in Tables 2-5, respectively.

Table 1. Parameters used in our model

m_q (GeV)	σ (GeV ²)	λ (GeV)	μ (GeV)	Λ (GeV)
4.744	4.967	0.240	0.039	0.17

Table 2. S wave mass spectra of $b\bar{b}$ states (in MeV)

States	Ours	Exp[67]	[46]	[54]	[59]	[57]	[74]
1^1S_0	9406.4	9398.7	9398	9402	9423	9412.22	9390
2^1S_0	9998.9	9999.0	9989	9976	9983	9995.48	9990
3^1S_0	10374.9		10336	10336	10342	10339.00	10326
4^1S_0	10671.8		10597	10635	10638	10572.49	10584
5^1S_0	10924.5		10810	10869	10901	10746.76	10800
6^1S_0	11147.9		10991	11097	11140	11064.47	10988
1^3S_1	9451.1	9460.3	9463	9465	9463	9460.75	9460
2^3S_1	10023.8	10023.3	10017	10003	10001	10026.22	10015
3^3S_1	10394.2	10355.1	10356	10354	10354	10364.65	10343
4^3S_1	10688.1	10579.4	10612	10635	10650	10594.47	10597
5^3S_1	10938.9	10885.2	10822	10878	10912	10766.14	10811
6^3S_1	11160.9	11000.0	11001	11102	11151	11081.70	10997

Table 3. P wave mass spectra of $b\bar{b}$ states (in MeV)

States	Ours	Exp[67]	[46]	[54]	[59]	[57]	[74]
1^1P_1	9872.9	9899.3	9894	9882	9899	9874.56	9909
2^1P_1	10271.7	10259.8	10259	10250	10268	10270.00	10254
3^1P_1	10582.7		10530	10541	10570	10526.50	10519
4^1P_1	10845.6		10751	10790		10714.80	
5^1P_1	11077.1		10938	11016		10863.00	
1^3P_0	9838.7	9859.4	9858	9847	9874	9849.61	9864
2^3P_0	10244.9	10232.5	10235	10226	10248	10252.54	10220
3^3P_0	10559.4		10513	10522	10551	10512.88	10490
4^3P_0	10824.5		10736	10775		10703.56	
5^3P_0	11057.4		10926	11004		10853.38	
1^3P_1	9865.7	9892.8	9889	9876	9894	9871.47	9903
2^3P_1	10266.2	10255.5	10255	10246	10265	10267.86	10249
3^3P_1	10578.1	10513.4	10527	10538	10567	10524.84	10515
4^3P_1	10841.5		10749	10788		10713.44	
5^3P_1	11073.3		10936	11014		10861.83	
1^3P_2	9885.6	9912.2	9910	9897	9907	9881.40	9921
2^3P_2	10282.3	10268.6	10269	10261	10274	10274.77	10264
3^3P_2	10592.3	10524.0	10539	10550	10576	10530.21	10528
4^3P_2	10854.6		10758	10798		10717.86	
5^3P_2	11085.6		10944	11022		10865.62	

Table 4. D wave mass spectra of $b\bar{b}$ states (in MeV)

States	Ours	Exp[67]	[46]	[54]	[59]	[57]	[74]
1^1D_2	10149.1		10163	10148	10149	10153.80	10153
2^1D_2	10476.3		10450	10450	10465	10456.60	10432
3^1D_2	10749.9		10681	10706	10740	10664.70	
4^1D_2	10989.2		10876	10935	10988	10823.00	
5^1D_2	11204.1		11046			10952.60	
1^3D_1	10139.4		10153	10138	10145	10144.99	10146
2^3D_1	10467.3		10442	10441	10462	10450.23	10425
3^3D_1	10741.3	10752.7	10675	10698	10736	10659.68	
4^3D_1	10981.0		10871	10928	10985	10818.83	
5^3D_1	11196.1		11041			10949.01	
1^3D_2	10147.9	10163.7	10162	10147	10149	10152.77	10153
2^3D_2	10475.0		10450	10449	10465	10455.86	10432
3^3D_2	10748.7		10681	10705	10740	10664.12	
4^3D_2	10987.9		10876	10934	10988	10822.52	
5^3D_2	11202.8		11045			10951.59	
1^3D_3	10154.2		10170	10155	10150	10158.31	10157
2^3D_3	10481.1		10456	10455	10466	10459.85	10436
3^3D_3	10754.6		10686	10711	10741	10667.25	
4^3D_3	10993.7		10880	10939	10990	10825.12	
5^3D_3	11208.5		11049			10954.42	

Table 5. F and G wave mass spectra of $b\bar{b}$ states (in MeV)

States	Ours	[46]	[54]	States	Ours	[46]	[54]
1^1F_3	10366.8	10366	10355	1^1G_4	10552.9	10534	10530
2^1F_3	10652.2	10609	10619	2^1G_4	10809.8	10747	10770
3^1F_3	10900.0	10812	10853	3^1G_4	11038.2	10929	
4^1F_3	11121.5	10988		4^1G_4	11245.3		
5^1F_3	11323.0			5^1G_4	11435.6		
1^3F_2	10363.6	10362	10350	1^3G_3	10552.8	10533	10529
2^3F_2	10648.8	10605	10615	2^3G_3	10809.2	10745	10769
3^3F_2	10896.5	10809	10850	3^3G_3	11037.3	10928	
4^3F_2	11117.8	10985		4^3G_3	11244.1		
5^3F_2	11319.2			5^3G_3	11434.3		
1^3F_3	10366.8	10366	10355	1^3G_4	10553.4	10535	10531
2^3F_3	10652.2	10609	10619	2^3G_4	10810.1	10747	10770
3^3F_3	10899.9	10812	10853	3^3G_4	11038.4	10929	
4^3F_3	11121.3	10988		4^3G_4	11245.5		
5^3F_3	11322.7			5^3G_4	11435.8		
1^3F_4	10368.5	10369	10358	1^3G_5	10552.6	10536	10532
2^3F_4	10654.1	10612	10622	2^3G_5	10809.8	10748	10772
3^3F_4	10902.1	10815	10856	3^3G_5	11038.5	10931	
4^3F_4	11123.7	10990		4^3G_5	11245.9		
5^3F_4	11325.3			5^3G_5	11436.4		

III. DECAY PROPERTIES

Bottomonium decays are important for understanding internal structures, revealing underlying dynamics, and distinguishing states. Comparison of mass spectra and decay properties with experimental data helps to validate theoretical models. Using the obtained wave functions, we calculate various decay properties of bottomonium.

Decay constants are fundamental parameters that characterize the strength of the weak interaction responsible for the decay processes, and it measures the probability amplitude to decay into lighter hadrons. The decay constant of pseudoscalar (f_P) and vector (f_V) states can be calculated using the Van Royen Weisskopf formula [47]

$$f_{P/V} = \sqrt{\frac{3|R_{P/V}(0)|^2}{\pi M_{P/V}}} \bar{C}(\alpha_s), \quad (19)$$

where $R_{P/V}(0)$ is the radial wavefunction at the origin for pseudoscalar (vector) meson state, $M_{P/V}$ is the mass of the pseudoscalar (vector) meson state and $\bar{C}(\alpha_s)$ is the QCD correction given by [48]

$$\bar{C}^2(\alpha_s) = 1 - \frac{\alpha_s(\mu)}{\pi} \left(\delta^P - \frac{m_q - m_{\bar{q}}}{m_q + m_{\bar{q}}} \ln \frac{m_q}{m_{\bar{q}}} \right), \quad (20)$$

where $\delta^P = 2$ and $\delta^V = 8/3$. The decay constant of P -wave states can be evaluated using [49, 50]

$$f_{\chi_0} = 12 \sqrt{\frac{3}{8\pi m_q}} \left(\frac{|R'_{\chi_0}(0)|}{M_{\chi_0}} \right),$$

$$f_{\chi_1} = 8 \sqrt{\frac{9}{8\pi m_q}} \left(\frac{|R'_{\chi_1}(0)|}{M_{\chi_1}} \right). \quad (21)$$

Here M_{χ_0} and M_{χ_1} are the masses of χ_0 and χ_1 states, respectively. The decay constants for pseudoscalar f_P and vector f_V are presented in Table 6 and decay constants for f_{χ_0} and f_{χ_1} are presented in Table 7. Bottomonium annihilation decays leave distinct signals in experimental data, allowing bottomonium states to be identified and characterized in high-energy collider experiments and precision spectroscopic investigations.

The leptonic decay formula for S -wave (n^3S_1) and D -wave (n^3D_1) states are calculated using Van Royen-Weisskopf formula along with the QCD correction factor [47, 51–53]

$$\Gamma(n^3S_1 \rightarrow l^+l^-) = \frac{4\alpha^2 e_q^2}{M(n^3S_1)^2} |R_{nS}(0)|^2 \left[1 - \frac{16\alpha_s(\mu)}{3\pi} \right],$$

$$\Gamma(n^3D_1 \rightarrow l^+l^-) = \frac{25\alpha^2 e_q^2}{2m_q^4 M(n^3D_1)^2} |R'_{nD}(0)|^2, \quad (22)$$

where $R'_{nL}(0)$ is the value of radial wavefunction at origin for nL state and $(')$ represents the order of derivative and $M(n^{2S+1}L_J)$ is the mass of $n^{2S+1}L_J$ state.

The annihilation decays for S -wave (n^1S_0) and P -wave (n^3P_0 and n^3P_2) into two photons ($\gamma\gamma$) and S -wave (n^3S_1) states into three photons ($\gamma\gamma\gamma$) with first order QCD correction factors are given by [51, 52]

$$\Gamma(n^1S_0 \rightarrow \gamma\gamma) = \frac{2^2 3\alpha^2 e_q^4}{M(n^1S_0)^2} |R_{nS}(0)|^2 \left[1 - \frac{3.4\alpha_s(\mu)}{\pi} \right],$$

$$\Gamma(n^3P_0 \rightarrow \gamma\gamma) = \frac{2^4 27\alpha^2 e_q^4}{M(n^3P_0)^4} |R'_{nP}(0)|^2 \left[1 + \frac{0.2\alpha_s(\mu)}{\pi} \right],$$

$$\Gamma(n^3P_2 \rightarrow \gamma\gamma) = \frac{2^4 36\alpha^2 e_q^4}{5M(n^3P_2)^4} |R'_{nP}(0)|^2 \left[1 - \frac{16\alpha_s(\mu)}{3\pi} \right],$$

$$\Gamma(n^3S_1 \rightarrow \gamma\gamma\gamma) = \frac{2^2 4(\pi^2 - 9)\alpha^3 e_q^6}{3\pi M(n^3S_1)^2} |R_{nS}(0)|^2 \left[1 - \frac{12.6\alpha_s(\mu)}{\pi} \right]. \quad (23)$$

The annihilation decays for S -wave (n^1S_0), P -wave (n^3P_0 and n^3P_2), D -wave (n^1D_2), F -wave (n^3F_2, n^3F_3 and n^3F_4) and G -wave (n^1G_4) states into two gluons (gg) with first order QCD correction factors are given by [51,

52, 54]

$$\begin{aligned}
\Gamma(n^1S_0 \rightarrow gg) &= \frac{2^2 2\alpha_s^2(\mu)}{3M(n^1S_0)^2} |R_{nS}(0)|^2 \left[1 + \frac{4.8\alpha_s(\mu)}{\pi} \right], \\
\Gamma(n^3P_0 \rightarrow gg) &= \frac{2^4 6\alpha_s^2(\mu)}{M(n^3P_0)^4} |R'_{nP}(0)|^2 \left[1 + \frac{10\alpha_s(\mu)}{\pi} \right], \\
\Gamma(n^3P_2 \rightarrow gg) &= \frac{2^4 8\alpha_s^2(\mu)}{5M(n^3P_2)^4} |R'_{nP}(0)|^2 \left[1 - \frac{0.1\alpha_s(\mu)}{\pi} \right], \\
\Gamma(n^1D_2 \rightarrow gg) &= \frac{2^6 2\alpha_s^2(\mu)}{3\pi M(n^1D_2)^6} |R''_{nD}(0)|^2 \left[1 - \frac{2.2\alpha_s(\mu)}{\pi} \right], \\
\Gamma(n^3F_2 \rightarrow gg) &= \frac{2^8 919\alpha_s^2(\mu)}{135M(n^3F_2)^8} |R'''_{nF}(0)|^2, \\
\Gamma(n^3F_3 \rightarrow gg) &= \frac{2^8 20\alpha_s^2(\mu)}{27M(n^3F_3)^8} |R'''_{nF}(0)|^2, \\
\Gamma(n^3F_4 \rightarrow gg) &= \frac{2^8 20\alpha_s^2(\mu)}{27M(n^3F_4)^8} |R'''_{nF}(0)|^2, \\
\Gamma(n^1G_4 \rightarrow gg) &= \frac{2^{10} 2\alpha_s^2(\mu)}{3\pi M(n^1G_4)^{10}} |R''''_{nG}(0)|^2.
\end{aligned} \tag{24}$$

The annihilation decays for S -wave (n^3S_1), P -wave (n^1P_1) and D -wave (n^3D_1, n^3D_2 and n^3D_3) states into three gluons (ggg) with first order QCD correction factors are given by [51, 52, 55]

$$\begin{aligned}
\Gamma(n^3S_1 \rightarrow ggg) &= \frac{2^2 10(\pi^2 - 9)\alpha_s^3(\mu)}{81\pi M(n^3S_1)^2} |R_{nS}(0)|^2 \left[1 - \frac{4.9\alpha_s(\mu)}{\pi} \right], \\
\Gamma(n^1P_1 \rightarrow ggg) &= \frac{2^4 20\alpha_s^3(\mu)}{9\pi M(n^1P_1)^4} |R'_{nP}(0)|^2 \ln(m_q \langle r \rangle), \\
\Gamma(n^3D_1 \rightarrow ggg) &= \frac{2^6 760\alpha_s^3(\mu)}{81\pi M(n^3D_1)^6} |R''_{nD}(0)|^2 \ln(4m_q \langle r \rangle), \\
\Gamma(n^3D_2 \rightarrow ggg) &= \frac{2^6 10\alpha_s^3(\mu)}{9\pi M(n^3D_2)^6} |R''_{nD}(0)|^2 \ln(4m_q \langle r \rangle), \\
\Gamma(n^3D_3 \rightarrow ggg) &= \frac{2^6 40\alpha_s^3(\mu)}{9\pi M(n^3D_3)^6} |R''_{nD}(0)|^2 \ln(4m_q \langle r \rangle).
\end{aligned} \tag{25}$$

The annihilation decays for S -wave (n^3S_1) states via strong and electromagnetic interaction, into a photon and two gluons (γgg) [44, 51, 56] and the P -wave (n^3P_1) into a light flavour meson and a gluon ($q\bar{q}g$) are given by [51, 52]

$$\begin{aligned}
\Gamma(n^3S_1 \rightarrow \gamma gg) &= \frac{2^2 8(\pi^2 - 9)e_q^2 \alpha_s^3(\mu)}{9\pi M(n^3S_1)^2} |R_{nS}(0)|^2 \\
&\quad \times \left[1 - \frac{7.4\alpha_s(\mu)}{\pi} \right], \\
\Gamma(n^3P_1 \rightarrow q\bar{q}g) &= \frac{2^4 8n_f \alpha_s^3(\mu)}{9\pi M(n^3P_1)^4} |R'_{nP}(0)|^2 \ln(m_q \langle r \rangle),
\end{aligned} \tag{26}$$

where n_f is the number of flavors. For all decays the strong coupling constant $\alpha_s(\mu)$ is calculated using the ex-

Table 6. Pseudoscalar and vector decay constants (in MeV)

States	$f_{P/V}$	Exp[67]	[59]	[57]	[80]	[81]
1^1S_0	655.9		529	578.21	646.025	744
2^1S_0	489.2		317	499.48	518.803	577
3^1S_0	431.8		280	450.35	474.954	511
4^1S_0	398.6		264	413.93	449.654	471
5^1S_0	375.5		255	385.68	432.072	443
6^1S_0	357.6		249	360.93	418.645	422
1^3S_1	640.2	715 ± 5	530	551.53	647.250	706
2^3S_1	478.0	498 ± 8	317	477.05	519.436	547
3^3S_1	422.0	430 ± 4	280	430.42	475.440	484
4^3S_1	389.7	336 ± 18	265	395.80	450.066	446
5^3S_1	349.7		255	368.91	432.437	419
6^3S_1	335.3		249	345.40	418.977	399

Table 7. Decay constants of P -wave states (in MeV)

States	f_{χ_0}	States	f_{χ_1}
1^3P_0	227.8	1^3P_1	262.4
2^3P_0	248.7	2^3P_1	286.6
3^3P_0	257.3	3^3P_1	296.6
4^3P_0	262.0	4^3P_1	302.1
5^3P_0	264.8	5^3P_1	305.4

pression

$$\alpha_s(\mu) = \frac{4\pi}{\beta_0 \ln \frac{\mu^2}{\Lambda^2}} \left[1 - \frac{\beta_1 \ln \left(\ln \frac{\mu^2}{\Lambda^2} \right)}{\beta_0^2 \ln \frac{\mu^2}{\Lambda^2}} \right], \tag{27}$$

where $\beta_0 = 11 - (2/3)n_f$, $\beta_1 = 102 - (18/3)n_f$, Λ is the QCD constant taken from [52], and μ is the reduced mass. All annihilation decay widths for $b\bar{b}$ bound system are presented in Tables 8-14, respectively.

The bottomonium states have substantially heavier masses and their intrinsic compactness is more pronounced [57]. As a result, radiative transitions in bottomonium are expected to be dominant because of the favourable conditions for photon emission or absorption [57]. Radiative transitions serves as an effective means to detect, especially for states with higher quantum numbers that are hard to observe with traditional techniques. The $E1$ radiative partial widths between the states ($n_i^{2S+1}L_i^i \rightarrow \gamma + n_f^{2S+1}L_f^f$) are given by [46, 58]

$$\Gamma_{E1}(i \rightarrow \gamma + f) = \frac{4\alpha e_q^2}{3} E_\gamma^3 \frac{E_f}{M_i} C_{fi} |\epsilon_{fi}|^2 \delta_{S_f S_i}. \tag{28}$$

Table 8. Di-leptonic decay widths (in keV for S states and in eV for D states)

States	Γ	Γ_{cf}	Exp[67]	[61]	[46]	[54]	[57]	[59]
1^3S_1	1.268	0.883	1.34±0.018	1.370	1.65	1.44	0.7700	0.582
2^3S_1	0.666	0.464	0.612±0.011	0.626	0.821	0.73	0.5442	0.197
3^3S_1	0.501	0.349	0.443±0.008	0.468	0.569	0.53	0.4288	0.149
4^3S_1	0.415	0.289	0.272±0.029	0.393	0.431	0.39	0.3549	0.129
5^3S_1	0.360	0.251	0.31±0.07	0.346	0.348	0.33	0.3035	0.117
6^3S_1	0.320	0.223	0.13±0.03	0.313	0.286	0.27	0.2586	0.109
1^3D_1	1.149			2.0	1.88	1.38	5.0	1.65
2^3D_1	2.166			3.0	2.81	1.99	5.8	2.42
3^3D_1	3.059			5.0	3.00	2.38	5.9	3.19
4^3D_1	4.573			6.0	3.00	2.18	5.8	3.97
5^3D_1	5.219			8.0	3.02		5.7	

Table 9. Di-photonic decay widths (in keV)

States	Γ	Γ_{cf}	[46]	[54]	[57]	[80]	[59]
1^1S_0	0.426	0.344	1.05	0.94	0.3035	0.387	0.2361
2^1S_0	0.223	0.180	0.489	0.41	0.2122	0.263	0.0896
3^1S_0	0.168	0.135	0.323	0.29	0.1668	0.229	0.0726
4^1S_0	0.139	0.112	0.237	0.20	0.1378	0.212	0.0666
5^1S_0	0.120	0.097	0.192	0.17	0.1176	0.201	0.0636
6^1S_0	0.107	0.086	0.152	0.14	0.1000	0.193	0.0619
1^3P_0	0.042	0.042	0.199	0.15	0.1150	0.0196	0.0168
2^3P_0	0.046	0.047	0.205	0.15	0.1014	0.0195	0.0172
3^3P_0	0.046	0.047	0.180	0.13	0.0875	0.0194	0.0192
4^3P_0	0.045	0.046	0.157	0.13	0.0768	0.0192	
5^3P_0	0.044	0.046	0.146		0.0686	0.0191	
1^3P_2	0.011	0.007	0.0106	0.0093	0.0147	0.0052	0.0024
2^3P_2	0.012	0.008	0.0133	0.012	0.0131	0.0052	0.0025
3^3P_2	0.012	0.009	0.0141	0.013	0.0114	0.0051	0.0027
4^3P_2	0.012	0.008	0.0142	0.015	0.0100	0.0051	
5^3P_2	0.011	0.008	0.0143		0.0090	0.0050	

Here $\alpha = 1/137$ is the fine structure constant, e_q is the quark charge, E_f is the energy of the final state, M_i is the mass of the initial state, $E_\gamma = (M_i^2 - M_f^2)/2M_i$ is the emitted photon energy. M_f is the mass of the final state. E_f/M_i is the relativistic phase factor and C_{fi} is the statistical factor given by

$$C_{fi} = \max(L_i, L_f) (2J_f + 1) \left\{ \begin{matrix} J_i & 1 & J_f \\ L_f & S & L_i \end{matrix} \right\}^2, \quad (29)$$

where $\{\{\{\}\}\}$ are the $6j$ symbol. In Eq. (28), ϵ_{fi} is the over-

Table 10. Tri-photonic decay widths (in 10^{-3} eV)

States	Γ	Γ_{cf}	[46]	[54]	[83]	[59]
1^3S_1	42.16	11.92	19.4	17.0	3.44	30.67
2^3S_1	22.17	6.27	10.9	9.8	2.00	11.58
3^3S_1	16.66	4.71	8.04	7.6	1.55	9.376
4^3S_1	13.81	3.91	6.36	6.0	1.29	8.590
5^3S_1	11.98	3.39	5.43		1.10	8.206
6^3S_1	10.65	3.01	4.57		0.96	7.982

Table 11. Di-gluonic decay widths of S , P (in MeV) and D (in keV) states

States	Γ	Γ_{cf}	[46]	[54]	[83]	[59]	[57]
1^1S_0	4.608	5.763	17.9	16.6	20.18	11.326	6.8520
2^1S_0	2.412	3.016	8.33	7.2	10.64	4.301	5.2374
3^1S_0	1.811	2.264	5.51	4.9	7.94	3.485	4.3182
4^1S_0	1.500	1.876	4.03	3.4		3.193	3.6829
5^1S_0	1.301	1.627	3.26			3.051	3.2196
6^1S_0	1.156	1.446	2.59			2.968	2.8519
1^3P_0	0.454	0.713	3.37	2.6	2.00	1.34	1.4297
2^3P_0	0.499	0.783	3.52	2.6	2.37	1.39	1.2358
3^3P_0	0.503	0.789	3.10	2.2	2.46	1.54	1.0539
4^3P_0	0.496	0.779	2.73	2.1			0.9175
5^3P_0	0.486	0.763	2.54				0.8127
1^3P_2	0.119	0.118	0.165	0.147	0.837	0.209	0.2370
2^3P_2	0.131	0.130	0.220	0.207	0.104	0.215	0.2064
3^3P_2	0.132	0.132	0.243	0.227	0.111	0.240	0.1767
4^3P_2	0.131	0.130	0.251	0.248			0.1543
5^3P_2	0.128	0.127	0.258				0.1370
1^1D_2	0.321	0.281	0.657	1.8	0.37	0.489	
2^1D_2	0.534	0.468	1.22	3.3	0.67	0.764	
3^1D_2	0.679	0.595	1.59	4.7		1.06	
4^1D_2	0.785	0.686	1.86			1.38	
5^1D_2	0.861	0.754	2.13				

lapping integral determined using the initial $R_{n_i l_i}(r)$ and final state $R_{n_f l_f}(r)$ wavefunctions:

$$\epsilon_{fi} = \frac{3}{E_\gamma} \int_0^\infty dr R_{n_i l_i}(r) R_{n_f l_f}(r) \left[\frac{E_\gamma r}{2} j_0 \left(\frac{E_\gamma r}{2} \right) - j_1 \left(\frac{E_\gamma r}{2} \right) \right] \quad (30)$$

The $M1$ radiative partial widths between the states ($n_i^{2S_i+1} L_{J_i} \rightarrow \gamma + n_f^{2S_f+1} L_{J_f}$) are given by [43, 58, 59]

$$\Gamma_{M1}(i \rightarrow \gamma + f) = \frac{4\alpha\mu_q^2}{3} \frac{2J_f + 1}{2L + 1} E_\gamma^3 \frac{E_f}{M_i} |m_{fi}|^2 \delta_{L_f L_i} \delta_{S_f S_i \pm 1}, \quad (31)$$

Table 12. Di-gluonic decay widths of F (in keV) and G (in eV) states

States	Γ	[46]	[54]	States	Γ	[46]	[54]
1^3F_2	0.282	0.834	0.70	1^3F_4	0.031	0.05	0.048
2^3F_2	0.618	2.04	1.77	2^3F_4	0.067	0.126	0.13
3^3F_2	0.946	3.17		3^3F_4	0.102	0.210	
4^3F_2	1.248			4^3F_4	0.135		
5^3F_2	1.517			5^3F_4	0.164		
1^3F_3	0.031	0.0672	0.060	1^1G_4	0.289	0.661	2.3
2^3F_3	0.067	0.167	0.16	2^1G_4	0.778		
3^3F_3	0.103	0.270		3^1G_4	1.383		
4^3F_3	0.135			4^1G_4	2.044		
5^3F_3	0.165			5^1G_4	2.723		

Table 13. Tri-gluonic decay widths (in keV)

States	Γ	Γ_{cf}	Exp[67]	[46]	[54]	[57]	[83]
1^3S_1	41.85	30.18	44.13±1.09	50.8	47.6	28.5	41.63
2^3S_1	22.00	15.86	18.8±1.59	28.4	26.3	19.3	24.25
3^3S_1	16.54	11.92	7.25±0.85	21.0	19.8	14.8	18.76
4^3S_1	13.71	9.89		16.7	15.1	12.1	15.58
5^3S_1	11.89	8.58		14.2	13.1	10.2	13.33
6^3S_1	10.57	7.62		12.0	11.0	8.5	11.57
1^1P_1	20.10			44.7	37.0	35.7	35.26
2^1P_1	26.99			64.6	54.0	34.6	52.70
3^1P_1	30.23			71.1	59.0	33.1	62.16
4^1P_1	31.99			73.2	64.0	32.7	
5^1P_1	32.97			76.2		30.9	
1^3D_1	3.11			10.4	8.11	10.6	9.97
2^3D_1	5.61			20.1	14.8	11.9	9.69
3^3D_1	7.54			26.0	21.2	11.8	
4^3D_1	9.05			30.4		11.3	
5^3D_1	1.02			34.7		10.8	
1^3D_2	0.37			0.821	0.69		0.62
2^3D_2	0.66			1.65	1.4		0.61
3^3D_2	0.89			2.27	2.0		
4^3D_2	0.11			2.75			
5^3D_2	0.12			3.23			
1^3D_3	1.46			2.19	2.07	6.0	0.22
2^3D_3	2.64			4.56	4.3	5.6	1.25
3^3D_3	3.54			6.65	6.6	5.5	
4^3D_3	4.26			8.38		5.3	
5^3D_3	4.82			10.1		5.1	

Table 14. Photo-gluon decay widths of S states and quark-gluon decay widths of P states (in keV)

States	Γ	Γ_{cf}	Exp[67]	[46]	[83]	[59]	[57]
1^3S_1	1.37	0.79	1.19±0.33	1.32	0.79	0.903	0.7220
2^3S_1	0.72	0.42	0.60±0.10	0.739	0.46	0.341	0.4982
3^3S_1	0.54	0.31	0.20±0.04	0.547	0.36	0.276	0.3874
4^3S_1	0.45	0.26		0.433	0.30	0.253	0.3176
5^3S_1	0.39	0.22		0.370	0.25	0.242	0.2698
6^3S_1	0.34	0.19		0.311	0.22	0.235	0.2272
1^3P_1	32.25			81.7	71.53	45.55	57.9585
2^3P_1	43.28			117.0	106.14	56.16	55.3966
3^3P_1	48.46			126.0	124.53	68.97	52.9585
4^3P_1	51.27			128.0			52.4466
5^3P_1	52.82			132.0			49.5181

where m_{fi} is given by

$$m_{fi} = \int_0^\infty dr R_{n_i l_i}(r) R_{n_f l_f}(r) \left[j_0 \left(\frac{E_\gamma r}{2} \right) \right], \quad (32)$$

and μ_q is the magnetic dipole moment given by [56]

$$\mu_q = \frac{m_{\bar{q}} e_q - m_q e_{\bar{q}}}{2m_q m_{\bar{q}}}. \quad (33)$$

The $E1$ transitions widths for S, P, D, F and G wave states are presented in Tables 15-19, respectively and the $M1$ transitions widths for S and P wave states are presented in Table 20.

IV. S-D MIXING

In bottomonium, the proximity of energy levels of higher excited states with same J^{PC} can result in mixing of states. The mixing is caused by the tensor potential term, but it is not strong enough to induce substantial mixing [60, 61]. However, for the states above open flavor threshold the mixing can be caused by coupled-channel dynamics, threshold effects, meson exchange, and multi-gluon exchange interactions [62–65]. These effects can modify the wavefunctions, causing mass shift and mixing between states, as well as affecting decay properties such as open channel strong decay, leptonic decays etc. Consequently, the conventional representation of bottomonium states as pure S and D wavefunctions breaks down, and the states are instead identified as admixtures of both components. The mixed states can be represented in terms of pure $|nS\rangle$ and $|n'D\rangle$ states as [61]

Table 15. $E1$ transition widths (in keV) and photon energies (in MeV) of S wave states

Initial State	Final State	Ours E_γ	Ours Γ_{E1}	Exp[67]	[46]	[54]	[83]	[74]
2^1S_0	1^1P_1	125.3	4.769		2.467	2.48	2.85	3.41
2^3S_1	1^3P_0	183.4	1.632	1.22 ± 0.11	0.907	0.91	1.09	1.09
	1^3P_1	156.9	3.092	2.21 ± 0.22	1.60	1.63	1.84	2.17
	1^3P_2	137.7	3.472	2.29 ± 0.22	1.86	1.88	2.08	2.62
3^1S_0	2^1P_1	102.7	6.596		2.88	2.96	2.60	4.25
	1^1P_1	489.9	0.226		1.12	1.3	0.0084	0.67
3^3S_1	2^3P_0	148.2	2.157	1.20 ± 0.12	1.06	1.03	1.21	1.21
	2^3P_1	127.2	4.132	2.56 ± 0.26	1.96	1.91	2.13	2.61
	2^3P_2	111.3	4.651	2.66 ± 0.27	2.37	2.30	2.56	3.16
	1^3P_0	540.6	0.057	0.055 ± 0.01	0.0099	0.01	0.15	0.097
	1^3P_1	515.1	0.115	0.018 ± 0.01	0.0363	0.05	0.16	0.0005
	1^3P_2	496.1	0.139	0.2 ± 0.03	0.359	0.45	0.0827	0.14
4^1S_0	3^1P_1	88.6	7.329		1.50	1.24		
	2^1P_1	392.5	0.718			0.732		
	1^1P_1	768.9	0.022		0.688			
4^3S_1	3^3P_0	127.9	2.384		0.587	0.48	0.61	
	3^3P_1	109.5	4.544		1.14	0.84	1.17	
	3^3P_2	95.4	5.057		1.16	0.82	1.45	
	2^3P_0	434.0	0.160		0.0137		0.17	
	2^3P_1	413.6	0.344		0.0138		0.18	
	2^3P_2	398.1	0.440		0.226		0.11	
	1^3P_0	815.7	0.007		5.12×10^{-4}		0.0588	
	1^3P_1	790.8	0.012		0.0507		0.0474	
	1^3P_2	772.4	0.013		0.219		0.012	

$$\begin{aligned}
|\phi\rangle &= \cos\theta|nS\rangle + \sin\theta|n'D\rangle, \\
|\phi'\rangle &= -\sin\theta|nS\rangle + \cos\theta|n'D\rangle,
\end{aligned} \tag{34}$$

where $|\phi\rangle$ and $|\phi'\rangle$ are the mixed states, and θ is the mixing angle. The masses of the mixed states can be calculated using [61]

$$\begin{aligned}
M_\phi &= \left[\left(\frac{M_{nS} + M_{n'D}}{2} \right) + \left(\frac{M_{nS} - M_{n'D}}{2 \cos 2\theta} \right) \right], \\
M_{\phi'} &= \left[\left(\frac{M_{nS} + M_{n'D}}{2} \right) + \left(\frac{M_{n'D} - M_{nS}}{2 \cos 2\theta} \right) \right].
\end{aligned} \tag{35}$$

Here M_ϕ and $M_{\phi'}$ are the masses of the mixed states, and M_{nS} and $M_{n'D}$ are the masses of the corresponding pure S and D states.

The leptonic decay widths of the mixed states are given by [61, 66]

Table 16. $E1$ transition widths (in keV) and photon energies (in MeV) of $1P$ and $2P$ wave states

Initial State	Final State	Ours E_γ	Ours Γ_{E1}	Exp[67]	[46]	[54]	[83]	[74]
1^1P_1	1^1S_0	455.4	38.692	35.77	34.4	35.7	43.66	35.8
1^3P_0	1^3S_1	379.9	23.099		22.8	23.8	28.07	27.5
1^3P_1	1^3S_1	405.8	27.901	32.544	28.3	29.5	35.66	31.9
1^3P_2	1^3S_1	424.9	31.805	34.38	31.4	32.8	39.15	31.8
2^1P_1	1^1D_2	121.8	3.604		1.81	1.7	5.36	2.24
	2^1S_0	269.1	21.962	40.32	15.0	14.1	17.60	16.2
	1^1S_0	828.8	11.071		10.8	13.0	14.90	16.1
2^3P_0	1^3D_1	104.9	2.316		1.05	1.0	0.74	1.77
	2^3S_1	218.7	12.165	1.2×10^{-4}	11.1	10.9	12.80	14.4
	1^3S_1	763.0	8.198		2.31	2.5	5.44	5.54
2^3P_1	1^3D_1	126.0	0.995		0.511	0.5	0.41	0.56
	1^3D_2	117.6	2.436		1.25	1.2	1.26	0.50
	2^3S_1	239.6	15.790	19.4 ± 5	13.7	13.3	15.89	15.3
	1^3S_1	782.7	8.991	8.9 ± 2.2	5.09	5.5	9.13	10.8
2^3P_2	1^3D_1	141.9	0.056		0.0267	0.03	0.0209	0.026
	1^3D_2	133.5	0.708		0.339	0.3	0.35	0.42
	1^3D_3	127.3	3.442		1.61	1.5	2.06	2.51
2^3S_1	2^3S_1	255.2	18.908	15.1 ± 5.6	14.6	14.3	17.50	15.3
1^3S_1	1^3S_1	797.6	9.626	9.8 ± 2.3	7.86	8.4	11.38	12.5

$$\begin{aligned}
\Gamma_\phi &= \left[\frac{2\alpha e_q}{M_{nS}} |R_{nS}(0)| \cos\theta + \frac{5\alpha e_q}{\sqrt{2}m_q^2 M_{n'D}} |R''_{n'D}(0)| \sin\theta \right]^2, \\
\Gamma_{\phi'} &= \left[\frac{5\alpha e_q}{\sqrt{2}m_q^2 M_{n'D}} |R''_{n'D}(0)| \cos\theta - \frac{2\alpha e_q}{M_{nS}} |R_{nS}(0)| \sin\theta \right]^2.
\end{aligned} \tag{36}$$

The leptonic decay of the mixed states is fitted to the experimental data to obtain the mixing angle, which is then used to calculate the masses of the mixed states. Our results of $S - D$ mixing are presented in Table 21.

V. RESULTS AND DISCUSSION

In this study, a screened potential model within a relativistic framework is employed to compute the mass spectrum and decay widths of $b\bar{b}$ bound system. The masses of S -wave states are presented in Table 2 and are compared with the experimental data and other theoretical models. The well-established $1S$ and $2S$ states serve as benchmarks, with our model predicting $\eta_b(1S) = 9406.4$ MeV, $\Upsilon(1S) = 9451.1$ MeV, $\eta_b(2S) = 9998.9$ MeV and $\Upsilon(2S) = 10023.8$ MeV. The hyperfine mass splitting given by $\Delta m(nS) = m[\Upsilon(nS)] - m[\eta_b(nS)]$, are evaluated to be $\Delta m(1S) = 44.7$ MeV and $\Delta m(2S) = 24.9$ MeV. These val-

Table 17. $E1$ transition widths (in keV) and photon energies (in MeV) of $3P$ states

Initial State	Final State	Ours E_γ	Ours Γ_{E1}	[46]	[54]	[83]	[74]
3^1P_1	2^1D_2	105.9	5.482	1.44	1.6	4.72	4.21
	1^1D_2	424.7	0.208	0.0585	0.081	0.35	0.17
	3^1S_0	205.8	18.156	9.94	8.9	12.27	14.1
	2^1S_0	567.7	7.175	4.60	8.2	6.86	7.63
	1^1S_0	1110.9	5.592	3.91	3.6	7.96	10.7
3^3P_0	2^3D_1	91.8	3.593	0.966	1.0	3.50	2.20
	1^3D_1	411.7	0.163	0.189	0.20	3.59×10^{-2}	0.15
	3^3S_1	163.9	9.527	7.15	6.9	8.50	7.95
	2^3S_1	522.0	5.156	1.26	1.7	2.99	2.55
	1^3S_1	1050.1	4.462	0.427	0.3	1.99	1.87
3^3P_1	2^3D_1	110.2	1.541	0.425	0.47	1.26	1.07
	2^3D_2	102.5	3.738	0.950	1.1	3.34	0.94
	1^3D_1	429.6	0.056	0.00418	7.0×10^{-3}	4.80×10^{-2}	0.010
	1^3D_2	421.4	0.147	0.0615	0.080	0.11	0.015
	3^3S_1	182.3	12.897	8.36	8.4	9.62	10.3
	2^3S_1	539.8	5.876	2.49	3.1	4.58	5.63
	1^3S_1	1066.9	4.754	1.62	1.3	4.17	6.41
	2^3D_1	124.3	0.088	0.0248	0.027	0.18	0.049
	2^3D_2	116.6	1.090	0.295	0.32	0.79	0.78
	2^3D_3	110.6	5.229	1.37	1.5	4.16	4.60
3^3P_2	1^3D_1	443.2	0.003	1.15×10^{-4}		3.38×10^{-3}	0.047
	1^3D_2	435.1	0.037	3.11×10^{-4}		4.41×10^{-2}	0.068
	1^3D_3	429.0	0.188	0.0288	0.046	0.21	0.12
	3^3S_1	196.2	15.889	9.30	9.3	10.38	10.8
	2^3S_1	553.2	6.478	3.66	4.5	5.62	6.72
	1^3S_1	1079.7	4.986	3.17	2.8	5.65	8.17

Table 18. $E1$ transition widths (in keV) and photon energies (in MeV) of D states

Initial State	Final State	Ours E_γ	Ours Γ_{E1}	[46]	[54]	[83]	[74]
1^1D_2	1^1P_1	272.5	28.719	24.3	24.9	17.23	30.3
1^3D_1	1^3P_0	296.3	20.292	16.3	16.5	20.98	19.8
	1^3P_1	270.0	11.661	9.51	9.7	12.29	13.3
1^3D_2	1^3P_2	250.6	0.626	0.550	0.56	0.65	1.02
	1^3P_1	278.3	22.890	18.8	19.2	21.95	21.8
1^3D_3	1^3P_2	258.9	6.194	5.49	5.6	6.23	7.23
	1^3P_2	265.1	26.518	23.9	24.3	24.74	32.1
2^1D_2	1^1F_3	108.9	2.640	1.35	1.8	2.20	
	2^1P_1	202.6	21.128	16.8	16.5	11.66	15.6
2^3D_1	1^1P_1	586.0	6.313	3.36	3.0	4.15	5.66
	1^3F_2	103.1	2.246	1.18	1.6	2.05	
2^3D_2	2^3P_0	220.0	14.846	11.0	10.6	8.35	9.58
	2^3P_1	199.1	8.380	6.71	6.5	4.84	6.74
2^3D_3	2^3P_2	183.3	0.441	0.40	0.4	0.24	0.47
	1^3P_0	609.7	4.118	2.99	2.9	3.52	5.56
2^3D_1	1^3P_1	584.3	2.599	1.03	0.9	1.58	2.17
	1^3P_2	565.5	0.152	0.030	0.02	0.061	0.44
2^3D_2	1^3F_2	110.8	0.308	0.164	0.21	0.24	
	1^3F_3	107.6	2.265	1.21	1.5	1.93	
2^3D_3	2^3P_1	206.7	16.793	13.1	12.7	9.10	11.4
	2^3P_2	190.9	4.462	3.96	3.8	2.55	3.75
2^3D_1	1^3P_1	591.6	4.921	2.81	2.6	3.43	4.00
	1^3P_2	572.9	1.441	0.489	0.4	0.80	1.11
2^3D_3	1^3F_2	116.8	0.007	0.004	0.005	0.005	
	1^3F_3	113.6	0.237	0.125	0.16	0.19	
2^3D_2	1^3F_4	112.0	2.632	1.37	1.7		
	2^3P_2	196.9	19.488	16.8	16.4	10.70	17.0
1^3P_2	1^3P_2	578.6	5.997	2.99	2.6	3.80	5.22

ues are consistent with the experimental results of $\Delta m(1S) = 62.3 \pm 3.2$ MeV and $\Delta m(2S) = 24.3 \pm 3.5_{-1.9}^{+2.8}$ MeV [67]. The $\Upsilon(10355)$ is well established as the $\Upsilon(3S)$ in the literature. In our model its mass is evaluated to be 10394.2 MeV. Our model predicts the mass difference $m[\Upsilon(3S)] - m[\Upsilon(2S)] = 370.4$ MeV compared to the experimental value of $331.50 \pm 0.02 \pm 0.13$ MeV [67]. The $\Upsilon(10580)$ is traditionally identified as the $\Upsilon(4S)$ state [46, 57, 59]. Our model calculates the mass of $\Upsilon(4S)$ as 10688.1 MeV which is overestimated by 108.7 MeV compared to experimental value. This overestimation is a consistent trend observed across all potential models [46, 59]. A 3P_0 model analysis suggests that $\Upsilon(10580)$ exhibits a significant meson-meson component due its proximity with the $B^* \bar{B}^*$ channel [68]. Ref. [69] suggests that the state discovered by the CLEO Collaboration at

$10684 \pm 10 \pm 8$ MeV, identified as a $b\bar{b}g$ hybrid [70], is a more suitable assignment for the $\Upsilon(4S)$ state, which is also corroborated by our model. The intermediate $B^* \bar{B}^*$ channel may induce observable $S - D$ mixing within the $\Upsilon(10580)$ state [68], and Ref. [61] predicts it to be $\Upsilon(4S) - \Upsilon(3D)$ mixture state with a substantial mixing angle. The $\Upsilon(10860)$ and $\Upsilon(11020)$ states are associated with the $\Upsilon(5S)$ and $\Upsilon(6S)$ states, respectively [46]. Our model predicts their masses as 10938.9 MeV and 11160.9 MeV, which are overestimated by 53.7 MeV and 160.9 MeV, respectively. Theoretical models commonly show discrepancies in $\Upsilon(5S)$ and $\Upsilon(6S)$ mass predictions, either overestimating or underestimating their values. Various interpretations have been explored in the literat-

Table 19. $E1$ transition widths (in keV) and photon energies (in MeV) of F and G states.

Initial State	Final State	Ours E_γ	Ours Γ_{E1}	[46]	[54]
1^1F_3	1^1D_2	215.3	27.505	22.0	18.8
1^3F_2	1^3D_1	221.8	25.149	19.4	16.4
	1^3D_2	213.4	4.171	3.26	2.7
	1^3D_3	207.3	0.109	0.0852	0.070
1^3F_3	1^3D_2	216.6	24.873	19.7	16.7
	1^3D_3	210.4	28.592	2.26	1.9
1^3F_4	1^3D_3	212.0	26.299	21.2	18.0
2^1F_3	1^1G_4	98.8	2.069	1.06	1.5
	2^1D_2	174.5	22.171	17.4	19.9
	1^1D_2	491.2	4.759	1.99	1.6
2^3F_2	1^3G_3	95.6	1.877	0.946	1.4
	2^3D_1	180.0	20.371	15.1	17.5
	2^3D_2	172.4	3.332	2.55	3.0
	2^3D_3	166.4	0.086	0.0681	0.080
	1^3D_1	497.2	4.214	1.95	1.6
	1^3D_2	489.1	0.727	0.224	0.16
	1^3D_3	483.1	0.019	0.00367	0.002
2^3F_3	1^3G_3	98.9	0.129	0.0664	0.10
	1^3G_4	98.2	1.910	0.957	1.4
	2^3D_2	175.6	20.091	15.4	17.9
	2^3D_3	169.7	2.275	1.80	2.1
	1^3D_2	492.3	4.273	1.83	1.4
	1^3D_3	486.3	0.506	0.145	0.1
2^3F_4	1^3G_3	100.8	0.002	8.80×10^{-4}	0.001
	1^3G_4	100.2	0.104	0.0535	0.080
	1^3G_5	100.9	2.098	1.05	1.5
	2^3D_3	171.6	21.148	16.9	19.6
	1^3D_3	488.2	4.635	0.126	1.4
1^1G_4	1^1F_3	184.5	27.129	21.1	23.1
1^3G_3	1^3F_2	187.5	26.098	20.1	22.3
	1^3F_3	184.3	2.174	1.67	1.8
	1^3F_4	182.7	0.034	0.0256	0.028
1^3G_4	1^3F_3	184.9	25.586	20.1	22.0
	1^3F_4	183.3	0.034	0.0256	0.028
1^3G_5	1^3F_4	182.6	26.304	21.1	23.1

Table 20. $M1$ transition widths (in keV) and photon energies (in MeV) of S and P states

Initial State	Final State	Ours E_γ	Ours Γ_{M1}	Exp[67]	[46]	[54]	[83]
1^3S_1	1^1S_0	44.5	4.228		9.52	10.0	9.34
2^1S_0	1^3S_1	532.8	4.848		70.6	68.0	45.0
2^3S_1	2^1S_0	24.8	0.732		0.582	0.590	0.580
	1^1S_0	598.3	3.569	12.5 ± 4.9	68.8	81.0	56.50
3^1S_0	2^3S_1	345.1	2.015		11.1	9.10	9.20
	1^3S_1	882.6	5.342		73.2	74.0	5.10
3^3S_1	3^1S_0	19.3	0.343		0.337	0.250	0.658
	2^1S_0	387.7	1.488	<13	11.8	19.0	11.0
	1^1S_0	940.8	2.836	10 ± 2	60.4	60.0	57.0
2^1P_1	1^3P_0	423.9	0.439		5.56	0.320	36.40
	1^3P_1	398.0	0.857		1.30	1.10	1.280
	1^3P_2	378.9	1.018		0.992	2.20	0.007
2^3P_0	1^1P_1	365.2	0.475		5.21	9.70	2.390
2^3P_1	1^1P_1	385.8	0.692		3.90×10^{-6}	2.20	0.167
2^3P_2	1^1P_1	401.2	0.905		3.86	0.240	1.780
3^1P_1	2^3P_0	332.5	0.366		2.16		1.710
	2^3P_1	311.8	0.709		0.559		0.597
	2^3P_2	269.2	0.831		0.407		0.007
	1^3P_0	717.9	0.279		5.10	0.980	3.770
	1^3P_1	692.8	0.639		1.01	0.930	1.230
	1^3P_2	674.2	0.867		1.48	0.140	0.051
3^3P_0	2^1P_1	283.4	0.372		2.05		
	1^1P_1	664.2	0.465		6.23		
3^3P_1	2^1P_1	301.9	0.569		9.80×10^{-4}		
	1^1P_1	681.7	0.566		0.032		
3^3P_2	2^1P_1	315.7	0.772		1.74		
	1^1P_1	694.9	0.654		3.53		

ure, where $\Upsilon(10860)$ is considered as mixture of $\Upsilon(5S) - P$ wave hybrid [71], while lattice QCD studies remain inconclusive on whether $\Upsilon(11020)$ corresponds to $\Upsilon(S)$ or $\Upsilon(D)$ state [72]. The 3P_0 model of Ref [68] concluded that $\Upsilon(10860)$ and $\Upsilon(11020)$ are structures are

mainly $b\bar{b}$ states with small $S - D$ mixing component. This was analyzed in Ref. [73], proposing $\Upsilon(10860)$ as a $\Upsilon(5S) - \Upsilon(4D)$ mixture, and in Ref. [61] it is suggested that both $\Upsilon(10860)$ and $\Upsilon(11020)$ are $\Upsilon(5S) - \Upsilon(4D)$ mixture. More experimental data is required to understand their nature. We discuss the possibility of $S - D$ mixing in $\Upsilon(10580)$, $\Upsilon(10860)$ and $\Upsilon(11020)$ later in this section.

The P -wave masses are presented in Table 3 and our evaluated masses for $1P$ and $2P$ states are in accordance with the experimental values. The experimentally determined mass difference are $m[\chi_{b2}(1P)] - m[\chi_{b1}(1P)] = 19.10 \pm 0.25$ MeV, $m[\chi_{b1}(1P)] - m[\chi_{b0}(1P)] = 32.49 \pm 0.93$ MeV, $m[\chi_{b2}(2P)] - m[\chi_{b1}(2P)] = 13.10 \pm 0.24$ MeV and $m[\chi_{b1}(2P)] - m[\chi_{b0}(2P)] = 23.8 \pm 1.7$ MeV [67]. Our model calculates these values as 19.9 MeV, 27 MeV, 16.1

Table 21. $S-D$ mixed states with the masses of mixed states M_ϕ and $M_{\phi'}$ (in MeV) and their di-leptonic decay widths Γ_ϕ and $\Gamma_{\phi'}$ (in keV)

$S-D$	M_S	θ	θ [61]	M_ϕ	M_{exp}	Γ_ϕ	Γ_{exp}
States	M_D			$M_{\phi'}$	[67]	$\Gamma_{\phi'}$	[67]
3S	10394.2	19.28	-9.0	10374.9	10355.1	0.440	0.443±0.008
2D	10467.3			10486.5		0.036	
4S	10688.1	-28.82	-12.5	10656.4	10579.4	0.272	0.272±0.029
3D	10741.3			10772.9	10752.7	0.129	
5S	10938.9	44.55	-38.0	10909.8	10885.2	0.291	0.31±0.07
4D	10981.0			11010.1	11000.0	0.142	0.13±0.03

MeV and 21.3 MeV, respectively, exhibiting good agreement with the experimental data. Among $3P$ bottomonium states, only $\chi_{b1}(3P)$ and $\chi_{b2}(3P)$ have been identified. In our model their masses are obtained as 10578.1 MeV and 10592.3 MeV, which are higher by 64.7 MeV and 68.9 MeV, respectively. This discrepancy can be due to proximity to open-flavor $B\bar{B}^*$ threshold, potentially causing mixing effects [75, 76]. The experimentally measured mass difference $m[\chi_{b2}(3P)] - m[\chi_{b1}(3P)] = 10.60 \pm 0.64 \pm 0.17$ MeV [67] is calculated as 14.2 MeV in our model. Masses of D -wave states are presented in Table 4.

The mass of $\Upsilon_1(1D)$ state in our model is evaluated to be 10147.9 MeV, deviating by 15.8 MeV from the experimental value [67]. The $\Upsilon_2(1D)$ and $\Upsilon_3(1D)$ states are estimated to have mass values of 10.13 GeV and 10.18 GeV, respectively [15], while our model calculates them as 10139.4 MeV and 10154.2 MeV, respectively. The recently observed $\Upsilon(10753)$ is generally associated with $\Upsilon_1(3D)$ [46, 76], although alternative interpretations suggest a tetraquark [77, 78], hybrid meson [3], etc. The mass of $\Upsilon_1(3D)$ state in our model is evaluated to be 10741.3 MeV, aligning with the experimental value [67]. A reanalysis of BABAR data estimated the mass of $\Upsilon_1(2D)$ to be 10495 ± 5 MeV with 10.7σ significance [79], while our model calculates it as 10467.3 MeV, showing consistency with experimental result. Masses of F and G -wave states are presented in Table 5. Our model shows consistency with other models for lower states, but deviations arise for higher excitations. The masses for different J states in Table 5 are very close to each other which could make it harder to differentiate these states experimentally.

Decay constants of pseudoscalar (f_P), vector (f_V) and tensor (f_{χ_0}, f_{χ_1}) states are presented in Tables 6 and 7, respectively. Our calculated values for the vector decay constants (f_V) are in accord with experimental values and shows more consistency over other theoretical models. The di-leptonic decay widths $\Gamma(l^+l^-)$ of $\Upsilon(nS)$ and $\Upsilon(nD)$

Table 22. Our assignments for $b\bar{b}$ states with masses (in MeV) and di-leptonic decay widths (in keV)

States	Assignment	M_{exp} [67]	M_{cal}	Γ_{exp}^{ee} [67]	Γ_{cal}^{ee}
$\eta_b(1S)$	$\eta_b(1S)$	9398.7±2	9406.4		
$\Upsilon(1S)$	$\Upsilon(1S)$	9460.4±0.09±0.04	9451.1	1.34±0.018	1.268
$\chi_{b0}(1P)$	$\chi_{b0}(1P)$	9859.44±0.42±0.31	9838.7		
$\chi_{b1}(1P)$	$\chi_{b1}(1P)$	9892.78±0.26±0.31	9865.7		
$h_b(1P)$	$h_b(1P)$	9899.3±0.8	9872.9		
$\chi_{b2}(1P)$	$\chi_{b2}(1P)$	9912.21±0.26±0.31	9885.6		
$\eta_b(2S)$	$\eta_b(2S)$	9999.0±3.5 ^{+2.8} _{-1.9}	9998.9		
$\Upsilon(2S)$	$\Upsilon(2S)$	10023.4±0.5	10023.3	0.612±0.011	0.666
$\Upsilon_2(1D)$	$\Upsilon_2(1D)$	10163.7±1.4	10147.9		
$\chi_{b0}(2P)$	$\chi_{b0}(2P)$	10232.5±0.4±0.5	10244.9		
$\chi_{b1}(2P)$	$\chi_{b1}(2P)$	10255.46±0.22±0.5	10266.2		
$h_b(2P)$	$h_b(2P)$	10259.8±0.5±1.1	10271.7		
$\chi_{b2}(2P)$	$\chi_{b2}(2P)$	10268.65±0.22±0.5	10282.3		
$\Upsilon(10355)$	$\Upsilon(3S) - \Upsilon(2D)$	10355.1±0.5	10374.9	0.443±0.008	0.440
$\chi_{b1}(3P)$	$\chi_{b1}(3P)$	10513.42±0.41±0.53	10578.1		
$\chi_{b2}(3P)$	$\chi_{b2}(3P)$	10524.02±0.57±0.53	10592.3		
$\Upsilon(10580)$	$\Upsilon(4S) - \Upsilon(3D)$	10579.4±1.2	10656.4	0.272±0.029	0.272
$\Upsilon(10753)$	$\Upsilon(4S) - \Upsilon(3D)$	10752.7±5.9 ^{+0.7} _{-1.1}	10772.9		0.129
$\Upsilon(10860)$	$\Upsilon(5S) - \Upsilon(4D)$	10885.2 ^{+2.6} _{-1.6}	10909.8	0.31±0.07	0.291
$\Upsilon(11020)$	$\Upsilon(5S) - \Upsilon(4D)$	11000±4	11010.1	0.13±0.03	0.142

states, without (Γ) and with (Γ_{cf}) the correction factor are presented in Table 8. The di-leptonic decay widths of $\Upsilon(nS)$ states evaluated without the correction term are more in agreement with the experimental value, while the correction factor significantly suppresses them. The di-leptonic decay widths of $\Upsilon(nD)$ are smaller than $\Upsilon(nS)$ by factor of 1000, serving as a key distinguishing feature in most models [46, 57]. The di-leptonic decay width difference between $\Upsilon(nS)$ and $\Upsilon(nD)$ states is used as a justification for assigning $\Upsilon(10580)$, $\Upsilon(10860)$, and $\Upsilon(11020)$ states to the $\Upsilon(4S)$, $\Upsilon(5S)$, and $\Upsilon(6S)$, respectively, in potential models. Since $\Upsilon(10580)$, $\Upsilon(10860)$ and $\Upsilon(11020)$ exhibit S state characteristics rather than being purely D state, their widths are often overestimated, suggesting a potential for $S-D$ mixing [61]. For $n \geq 3$ the probability of $S-D$ mixing increases and even a small mixing angle can increase the di-leptonic decay widths of $\Upsilon(nD)$ by order of 2 [82]. To study $S-D$ mixing in our model, the di-leptonic decay widths without the correction factor are utilized to obtain the mixing angle. The diphotonic decay widths $\Gamma(\gamma\gamma)$ of bottomonium states without (Γ) and with (Γ_{cf}) the correction factor are listed in Table 9. Our results are comparable to Ref. [57, 80] in magnitude, but are lower than those in Ref. [46, 54]. The di-photon decay width of $\eta_b(1S)$ is not seen experimentally and we predict it to be 0.344 keV. The tri-photon decay widths $\Gamma(\gamma\gamma\gamma)$ without (Γ) and with (Γ_{cf}) the correction factor are listed in Table 10. The values of tri-photon decay widths vary significantly among models, highlighting the need for experimental validation. The di-gluonic decay widths $\Gamma(gg)$ without (Γ) and with (Γ_{cf}) the correction factor are calculated in Table 11 and Table 12. Our di-gluonic decay widths of S , P and D states are comparable to [57] but are 2-4 times smaller than those in [46, 54, 59, 83]. For lower-lying $\eta_b(nS)$ states, the di-gluonic decay widths constitute approximately $\sim 100\%$ of their total width due to suppression of OZI-allowed two-body strong decays [46]. Our evaluated di-gluonic width for $\eta_b(1S)$ is 5.763, close to the lower limit of total width estimate of 10.0^{+5}_{-4} MeV [67]. The tri-gluonic decay widths $\Gamma(ggg)$ without (Γ) and with (Γ_{cf}) the correction factor are presented in Table 13. The tri-gluonic decay width for $\Upsilon(1S)$ is lower by 13.95 MeV, while those for $\Upsilon(2S)$ and $\Upsilon(3S)$ agree well with experimental results. For P and D states, our predicted widths are lower than other models. The photo-gluonic decay widths $\Gamma(\gamma gg)$ and quark-gluonic decay width $\Gamma(q\bar{q}g)$ without (Γ) and with (Γ_{cf}) the correction factor are evaluated in Table 14. The photo-gluonic decay widths of $\Upsilon(1S)$, $\Upsilon(2S)$ and $\Upsilon(3S)$ are in accordance with the experimental data. The multi-gluon or hybrid $q\bar{q}g$ decays are dominant channel for $\chi_{b1}(1P)$ state [46]. Our predictions for quark-gluonic decay width for $\chi_{b1}(1P)$ are observed to be lower compared to other models.

The S wave $E1$ transitions widths are calculated in

Table 15. The transition widths $\Gamma(2S \rightarrow \gamma\chi_b(1P))$ in our model align well with experimental data. The transition widths for $\Gamma(\Upsilon(3S) \rightarrow \gamma\chi_b(P))$ presents a complex scenario, due to discrepancies in $\Gamma(\Upsilon(3S) \rightarrow \gamma\chi_b(2P))$ and $\Gamma(\Upsilon(3S) \rightarrow \gamma\chi_b(1P))$ predictions across models [46, 83]. Our model estimates $\Gamma(\Upsilon(3S) \rightarrow \gamma\chi_b(2P))$ slightly higher than experimental values, while $\Gamma(\Upsilon(3S) \rightarrow \gamma\chi_b(1P))$ are highly suppressed, a typical feature of $E1$ transitions among states separated by two radial nodes, making them susceptible to relativistic corrections [84, 85]. This suppression is evident in our evaluation, where $\Gamma(\Upsilon(3S) \rightarrow \gamma\chi_{b0}(1P)) = 0.057$ keV and $\Gamma(\Upsilon(3S) \rightarrow \gamma\chi_{b2}(1P)) = 0.139$ align with experimental results, while $\Gamma(\Upsilon(3S) \rightarrow \gamma\chi_{b1}(1P)) = 0.115$ keV exceeds the experimental value. This atypical hierarchy of $\Gamma(\Upsilon(3S) \rightarrow \gamma\chi_{b2}(1P)) > \Gamma(\Upsilon(3S) \rightarrow \gamma\chi_{b0}(1P)) > \Gamma(\Upsilon(3S) \rightarrow \gamma\chi_{b1}(1P))$ mentioned in Ref. [86] is also observed in our model. This is attributed to $\chi_{b1}(1P)$ mixing with $\chi_b(2P)$ and $\chi_b(3P)$, further suppressing $\Gamma(\Upsilon(3S) \rightarrow \gamma\chi_{b1}(1P))$. In Ref. [61], the $S-D$ mixing in $\Upsilon(3S)$ is considered to explain the $E1$ transitions widths of $\Gamma(\Upsilon(3S) \rightarrow \gamma\chi_b(2P))$, which allowed them to reproduce the experimental widths. This explanation may also be extended for analysis of $\Gamma(\Upsilon(3S) \rightarrow \gamma\chi_b(1P))$ transition widths. We also evaluate the $\Gamma(4S \rightarrow \gamma P)$. The P wave $E1$ transitions widths are presented in Table 16 and 17. The transition width $\Gamma(1P \rightarrow \gamma S)$ in our model agrees with the experimental and theoretical results. Using the measured branching ratios $B[\chi_{b0}(1P) \rightarrow \gamma\Upsilon(1S)] = 1.94 \pm 0.27\%$, $B[\chi_{b1}(1P) \rightarrow \gamma\Upsilon(1S)] = 35.2 \pm 2.0\%$, and $B[\chi_{b2}(1P) \rightarrow \gamma\Upsilon(1S)] = 18.0 \pm 1.0\%$ [67], we calculate the total decay width as 1.19 MeV for $\chi_{b0}(1P)$, 79.0 keV for $\chi_{b1}(1P)$, and 177.0 keV for $\chi_{b2}(1P)$. Our total width for $\chi_{b0}(1P)$ is consistent with 1.3 ± 0.9 MeV and $\Gamma_{total} < 2.4$ MeV condition predicted by Belle Collaboration [87]. The $h_b(1P)$ has primary transition $h_b(1P) \rightarrow \gamma\eta_b(1S)$ with measured branching ratio of $52^{+6}_{-5}\%$. Using this, we estimate the total decay width of $h_b(1P)$ as 74.0 keV, consistent with the Ref. [74]. The evaluated transition width $h_b(2P) \rightarrow \gamma\eta_b(2S)$ is lower than the experimental value, a trend seen in most of the potential models. Using measured branching ratios $B[h_b(2P) \rightarrow \gamma\eta_b(2S)] = 48 \pm 13\%$ and $B[h_b(2P) \rightarrow \gamma\eta_b(1S)] = 22 \pm 5\%$ [67], we estimate the total decay width of $h_b(2P)$ as 46.0 keV and 50.0 keV, respectively, with an average of 48.0 keV, which is smaller than the estimate in Ref. [74]. The transition width $\Gamma(\chi_{b0}(1P) \rightarrow \gamma\Upsilon(2S))$ is overestimated in most models. From the measured branching ratios $B[\chi_{b0}(2P) \rightarrow \gamma\Upsilon(2S)] = 1.38 \pm 0.30\%$ and $B[\chi_{b0}(2P) \rightarrow \gamma\Upsilon(1S)] = (3.8 \pm 1.7) \times 10^{-3}$ [67], we determine the total decay width of $\chi_{b0}(2P)$ as 0.88 MeV and 2.20 MeV, respectively. While these values vary significantly, the latter aligns with the (~ 2.5 MeV) prediction of Ref. [54]. Our model predicts $\Gamma(\chi_{b1}(2P) \rightarrow \gamma\Upsilon(S))$ and $\Gamma(\chi_{b2}(2P) \rightarrow \gamma\Upsilon(S))$ in excellent agreement with experimental results. Using

measured branching ratios $B[\chi_{b1}(2P) \rightarrow \gamma\Upsilon(2S)] = 18.1 \pm 1.9\%$ and $B[\chi_{b1}(2P) \rightarrow \gamma\Upsilon(1S)] = 9.9 \pm 1.0\%$ [67], we determine the total decay width of $\chi_{b1}(2P)$ as 87.0 keV and 91.0 keV, respectively, with an average of 89.0 keV, which aligns with the CLEO Collaboration value 96 ± 16 keV [88]. Using the branching ratio $B[\chi_{b2}(2P) \rightarrow \gamma\Upsilon(1S)] = 6.6 \pm 0.8\%$ [67], we calculate the decay width of 146.0 ± 18.0 keV for $\chi_{b2}(2P)$, which agrees with 138 ± 19 keV obtained by CLEO Collaboration [88]. No experimental data exists for $\Gamma(3P \rightarrow \gamma S)$ and $\Gamma(3P \rightarrow \gamma D)$ transitions, although detections of $\Gamma(\chi_{b1}(3P) \rightarrow \gamma\Upsilon(1S))$, $\Gamma(\chi_{b1}(3P) \rightarrow \gamma\Upsilon(2S))$, $\Gamma(\chi_{b1}(3P) \rightarrow \gamma\Upsilon(3S))$, and $\Gamma(\chi_{b2}(3P) \rightarrow \gamma\Upsilon(3S))$ have been reported. We estimate these transition widths as 4.754 keV, 5.876 keV, 12.895 keV, and 15.899 keV, respectively. $E1$ transition widths for D -wave states are presented in Table 18. The transition $\Gamma(\Upsilon_2(1D) \rightarrow \gamma\chi_b(1P))$ has been observed [67] and our model estimates $\Gamma(\Upsilon_2(1D) \rightarrow \gamma\chi_{b2}(1P)) = 6.194$ keV and $\Gamma(\Upsilon_2(1D) \rightarrow \gamma\chi_{b1}(1P)) = 22.890$ keV are consistent with other theoretical models. Ref. [46, 54, 83] suggest the total decay widths of $\eta_b(1D)$ and $\Upsilon_3(1D)$ are equivalent to their transition widths $\Gamma(\eta_b(1D) \rightarrow \gamma h_b(1P))$ and $\Gamma(\Upsilon_3(1D) \rightarrow \gamma h_b(1P))$, respectively. We estimate these transition widths to be 28.719 keV and 26.518 keV, respectively, in accordance with other models. The $\Upsilon_1(1D)$ state is predicted to be detected in $\Gamma(\Upsilon_1(1D) \rightarrow \gamma\chi_{b0}(1P))$ and $\Gamma(\Upsilon_1(1D) \rightarrow \gamma\chi_{b1}(1P))$ due to their large branching ratios [46, 54, 83]. Our model estimates these transition widths as 20.292 keV and 11.661 keV, respectively. The large branching ratio of $\Gamma(\eta_b(2D) \rightarrow \gamma h_b(2P))$ suggests that the unobserved $\eta_b(2D)$ state could be detected [46, 54]. Our model estimates $\Gamma(\eta_b(2D) \rightarrow \gamma h_b(2P))$ to be 21.128 keV. The transition widths of $2D$ states in our model align with other theoretical predictions. $E1$ transition widths for F and G wave states are listed in Table 19, which are slightly higher than those in other potential models. The $M1$ transition widths are presented in Table 20. Our $M1$ transition widths show noticeable differences from Refs. [46, 54, 57]. While our $\Gamma(\Upsilon(nS) \rightarrow \gamma\eta_b(nS))$ estimates are lower than other models, they aligns more closely with experimental results. Since decay widths are highly dependent on the wavefunction, estimates vary significantly across models.

Table 21 presents the masses and leptonic decay widths of $S - D$ mixed states, which are assigned to experimentally observed states. The $\Upsilon(10355)$ state is considered as $3S - 2D$ mixed state with a small mixing component, having mass of 10374.9 MeV and leptonic width

of 0.440 keV. The $\Upsilon(10580)$ and $\Upsilon(10753)$ are considered to be $4S - 3D$ mixed state with substantial mixing component, with mass of 10656.4 MeV and leptonic width of 0.272 keV for $\Upsilon(10580)$ and mass of 10772.9 MeV and leptonic width of 0.129 keV for $\Upsilon(10753)$. The $\Upsilon(10860)$ and $\Upsilon(11020)$ are assigned to be $5S - 4D$ mixed states, which is also supported by Ref. [61]. The mass and leptonic decay width values of the $\Upsilon(10860)$ and $\Upsilon(11020)$ are consistent with the experimental results. After taking into account the $S - D$ mixing, our final assignments are presented in Table 22.

VI. CONCLUSION

In this study, we explored the bottomonium system using a screened potential model within a relativistic framework to compute the mass spectrum of S, P, D, F and G wave, decay widths, and $E1$ and $M1$ transition widths, along with mass and leptonic decay widths of $S - D$ mixed states. This study emphasizes the relevance of relativistic dynamics, screening, and state mixing, offering a framework that bridges gaps between theory and experiment. The computed mass values exhibit strong agreement with experimental data, particularly for lower states, while our predictions for higher excited states demonstrate notable improvements compared to previous potential models. A recurring challenge in bottomonium spectroscopy has been reconciling theoretical predictions with experimental measurements, particularly for the masses and leptonic decay widths of higher states such as $\Upsilon(10355)$, $\Upsilon(10580)$, $\Upsilon(10860)$ and $\Upsilon(11020)$. Our study addresses this by incorporating $S - D$ mixing, yielding results that align closely with experimental values and providing a more refined interpretation of these states and emphasizing the need for beyond-static-potential effects in quarkonium spectroscopy. Our calculations of decay constants, particularly for vector states, show improvements over prior models along with annihilation decay widths. Beyond mass spectra, our evaluation of $E1$ and $M1$ transition widths offers valuable insights into radiative decays, supporting experimental searches for unobserved bottomonium states. We also utilized $E1$ transition widths to estimate the total decay widths of higher bottomonium states, achieving reasonable agreement with experimental values and reinforcing the validity of our model. Additionally, the calculated transition widths for higher excited states serve as references. This research paves the way for future investigations, particularly in the exploration of higher excited states and the effects of $S - D$ mixing.

References

- [1] F.-K. Guo, H. Peng, J.-J. Xie, and X. Zhou, arXiv 10.48550/arXiv.2203.07141 (2022), 2203.07141.
- [2] D. M. Asner, H. Atmacan, S. Banerjee, J. V. Bennett, M. Bertemes, *et al.*, arXiv 10.48550/arXiv.2203.10203 (2022),

- 2203.10203.
- [3] N. Brambilla, S. Eidelman, C. Hanhart, A. Nefediev, C.-P. Shen, *et al.*, *Phys. Rep.* **873**, 1 (2020)
- [4] S. W. Herb, D. C. Hom, L. M. Lederman, J. C. Sens, H. D. Snyder, *et al.*, *Phys. Rev. Lett.* **39**, 252 (1977)
- [5] W. R. Innes, J. A. Appel, B. C. Brown, C. N. Brown, K. Ueno, *et al.*, *Phys. Rev. Lett.* **39**, 1240 (1977)
- [6] K. Han, T. Böhringer, P. Franzini, G. Mageras, D. Peterson, *et al.*, *Phys. Rev. Lett.* **49**, 1612 (1982)
- [7] G. Eigen, G. Blunar, H. Dietl, E. Lorenz, F. Pauss, *et al.*, *Phys. Rev. Lett.* **49**, 1616 (1982)
- [8] C. Klopfenstein, J. E. Horstkotte, J. Lee-Franzini, R. D. Schamberger, M. Sivertz, *et al.*, *Phys. Rev. Lett.* **51**, 160 (1983)
- [9] F. Pauss, H. Dietl, G. Eigen, E. Lorenz, G. Mageras, *et al.*, *Phys. Lett. B* **130**, 439 (1983)
- [10] CLEO Collaboration, M. Artuso, C. Boulahouache, S. Blusk, J. Butt, *et al.*, *Phys. Rev. Lett.* **94**, 032001 (2005)
- [11] D. Andrews, K. Berkelman, R. Cabenda, D. G. Cassel, J. W. DeWire, *et al.*, *Phys. Rev. Lett.* **45**, 219 (1980)
- [12] D. Besson, J. Green, R. Namjoshi, F. Sannes, P. Skubic, *et al.*, *Phys. Rev. Lett.* **54**, 381 (1985)
- [13] R. Mizuk, A. Bondar, I. Adachi, H. Aihara, D. M. Asner, *et al.*, *J. High Energy Phys.* **2019**(10), 1
- [14] G. Bonvicini, D. Cinabro, M. Dubrovin, A. Bornheim, E. Lipeles, *et al.*, *Phys. Rev. D* **70**, 032001 (2004)
- [15] BABAR Collaboration, P. del Amo Sanchez, J. P. Lees, V. Poireau, E. Prencipe, *et al.*, *Phys. Rev. D* **82**, 111102 (2010)
- [16] BABAR Collaboration, B. Aubert, M. Bona, Y. Karyotakis, J. P. Lees, *et al.*, *Phys. Rev. Lett.* **101**, 071801 (2008)
- [17] S. Dobbs, Z. Metreveli, A. Tomaradze, T. Xiao, and K. K. Seth, *Phys. Rev. Lett.* **109**, 082001 (2012)
- [18] S. Dobbs and The CLEO Collaboration, AIP Conf. Proc. **1257**, 408 (2010)
- [19] Belle Collaboration, R. Mizuk, D. M. Asner, A. Bondar, T. K. Pedlar, *et al.*, *Phys. Rev. Lett.* **109**, 232002 (2012)
- [20] The BABAR Collaboration, J. P. Lees, V. Poireau, E. Prencipe, V. Tisserand, *et al.*, *Phys. Rev. D* **84**, 091101 (2011)
- [21] Belle Collaboration, I. Adachi, H. Aihara, K. Arinstein, D. M. Asner, *et al.*, *Phys. Rev. Lett.* **108**, 032001 (2012)
- [22] ATLAS Collaboration, G. Aad, B. Abbott, J. Abdallah, A. A. Abdelalim, *et al.*, *Phys. Rev. Lett.* **108**, 152001 (2012)
- [23] D0 Collaboration, V. M. Abazov, B. Abbott, B. S. Acharya, M. Adams, *et al.*, *Phys. Rev. D* **86**, 031103 (2012)
- [24] CMS Collaboration, A. M. Sirunyan, A. Tumasyan, W. Adam, F. Ambrogio, *et al.*, *Phys. Rev. Lett.* **121**, 092002 (2018)
- [25] Belle Collaboration, A. Bondar, A. Garmash, R. Mizuk, D. Santel, *et al.*, *Phys. Rev. Lett.* **108**, 122001 (2012)
- [26] F.-K. Guo, C. Hanhart, U.-G. Meißner, Q. Wang, Q. Zhao, *et al.*, *Rev. Mod. Phys.* **90**, 015004 (2018)
- [27] Q. Wang, V. Baru, A. A. Filin, C. Hanhart, A. V. Nefediev, *et al.*, *Phys. Rev. D* **98**, 074023 (2018)
- [28] E. S. Swanson, *Phys. Rev. D* **91**, 034009 (2015)
- [29] L. Maiani, A. D. Polosa, and V. Riquer, *Phys. Lett. B* **778**, 247 (2018)
- [30] R. Mizuk, A. Bondar, I. Adachi, H. Aihara, D. M. Asner, *et al.*, *J. High Energy Phys.* **2019**(10), 1
- [31] X.-K. Dong, X.-H. Mo, P. Wang, and C.-Z. Yuan, *Chin. Phys. C* **44**, 083001 (2020)
- [32] W.-S. Hou, *Phys. Rev. D* **74**, 017504 (2006)
- [33] A. Ali, C. Hambrock, I. Ahmed, and M. J. Aslam, *Phys. Lett. B* **684**, 28 (2010)
- [34] F.-K. Guo, C. Hidalgo-Duque, J. Nieves, and M. Pavxon Valderrama, *Phys. Rev. D* **88**, 054007 (2013)
- [35] G. Mezzadri and S. Spataro, *Rev. Phys.* **8**, 100070 (2022)
- [36] C. A. Bokade and Bhaghyesh, *Phys. Rev. D* **111**, 014030 (2025)
- [37] S. Godfrey and N. Isgur, *Phys. Rev. D* **32**, 189 (1985)
- [38] D. Yibing, C. Kuangta, and Q. Danhua, *Chin. Phys. Lett.* **10**, 460 (1993)
- [39] J.-B. Liu and M.-Z. Yang, *J. High Energy Phys.* **2014**(7), 1
- [40] M.-Z. Yang, *Eur. Phys. J. C* **72**, 1 (2012)
- [41] E. Eichten and F. Feinberg, *Phys. Rev. D* **23**, 2724 (1981)
- [42] M. B. Voloshin, *Prog. Part. Nucl. Phys.* **61**, 455 (2008)
- [43] T. Barnes, S. Godfrey, and E. S. Swanson, *Phys. Rev. D* **72**, 054026 (2005)
- [44] R. F. Lebed and E. S. Swanson, *Phys. Rev. D* **96**, 056015 (2017)
- [45] B.-Q. Li and K.-T. Chao, *Phys. Rev. D* **79**, 094004 (2009)
- [46] J.-Z. Wang, Z.-F. Sun, X. Liu, and T. Matsuki, *Eur. Phys. J. C* **78**, 1 (2018)
- [47] R. Van Royen and V. F. Weisskopf, *Nuovo Cimento A (1965-1970)* **50**, 617 (1967)
- [48] E. Braaten and S. Fleming, *Phys. Rev. D* **52**, 181 (1995)
- [49] J. P. Lansberg and T. N. Pham, *Phys. Rev. D* **79**, 094016 (2009)
- [50] N. Akbar, *J. Korean Phys. Soc.* **77**, 17 (2020)
- [51] W. Kwong and J. L. Rosner, *Phys. Rev. D* **38**, 279 (1988)
- [52] W. Kwong, P. B. Mackenzie, R. Rosenfeld, and J. L. Rosner, *Phys. Rev. D* **37**, 3210 (1988)
- [53] V. A. Novikov, L. B. Okun, M. A. Shifman, A. I. Vainshtein, M. B. Voloshin, *et al.*, *Phys. Rep.* **41**, 1 (1978)
- [54] S. Godfrey and K. Moats, *Phys. Rev. D* **92**, 054034 (2015)
- [55] G. Bxelanger and P. Moxhay, *Phys. Lett. B* **199**, 575 (1987)
- [56] W. A. Bardeen, E. J. Eichten, and C. T. Hill, *Phys. Rev. D* **68**, 054024 (2003)
- [57] B. Pandya, M. Shah, and P. C. Vinodkumar, *Eur. Phys. J. C* **81**, 1 (2021)
- [58] E. Eichten, K. Gottfried, T. Kinoshita, K. D. Lane, and T.-M. Yan, *Phys. Rev. D* **17**, 3090 (1978)
- [59] V. Kher, R. Chaturvedi, N. Devlani, and A. K. Rai, *Eur. Phys. J. Plus* **137**, 1 (2022)
- [60] S. F. Radford and W. W. Repko, *Phys. Rev. D* **75**, 074031 (2007)
- [61] Z. Zhao, K. Xu, A. Limphirat, W. Sreethawong, N. Tagsinsit, *et al.*, *Phys. Rev. D* **109**, 016012 (2024)
- [62] K. Heikkilä, N. A. Törnqvist, and S. Ono, *Phys. Rev. D* **29**, 110 (1984)
- [63] Y. Lu, M. N. Anwar, and B.-S. Zou, *Phys. Rev. D* **94**, 034021 (2016)
- [64] R. Machleidt, K. Holinde, and Ch. Elster, *Phys. Rep.* **149**, 1 (1987)
- [65] L. Ya. Glozman and D. O. Riska, *Phys. Rep.* **268**, 263 (1996)
- [66] J.-Z. Wang and X. Liu, *Phys. Lett. B* **849**, 138456 (2024)
- [67] Particle Data Group, R. L. Workman, V. D. Burkert, V. Crede, E. Klempt, *et al.*, *Prog. Theor. Exp. Phys.* **2022**, 083C01 (2022)
- [68] W.-H. Liang, N. Ikeno, and E. Oset, *Phys. Lett. B* **803**, 135340 (2020)
- [69] E. van Beveren and G. Rupp, *Phys. Rev. D* **80**, 074001 (2009)
- [70] D. Besson, J. Green, R. Namjoshi, F. Sannes, P. Skubic, *et al.*, *Phys. Rev. Lett.* **54**, 381 (1985)

- [71] R. Bruschini and P. Gonzxalez, *Phys. Lett. B* **791**, 409 (2019)
- [72] P. Bicudo, N. Cardoso, L. Mueller, and M. Wagner, *Phys. Rev. D* **107**, 094515 (2023)
- [73] Q. Li, M.-S. Liu, Q.-F. Lü, L.-C. Gui, and X.-H. Zhong, *Eur. Phys. J. C* **80**, 1 (2020)
- [74] W.-J. Deng, H. Liu, L.-C. Gui, and X.-H. Zhong, *Phys. Rev. D* **95**, 074002 (2017)
- [75] M. Karliner and J. L. Rosner, *Phys. Rev. D* **91**, 014014 (2015)
- [76] B. Chen, A. Zhang, and J. He, *Phys. Rev. D* **101**, 014020 (2020)
- [77] A. Ali, L. Maiani, A. Y. Parkhomenko, and W. Wang, *Phys. Lett. B* **802**, 135217 (2020)
- [78] Z.-G. Wang, *Chin. Phys. C* **43**, 123102 (2019)
- [79] E. van Beveren and G. Rupp, arXiv 10.48550/arXiv.1009.4097 (2010), 1009.4097.
- [80] N. R. Soni, B. R. Joshi, R. P. Shah, H. R. Chauhan, and J. N. Pandya, *Eur. Phys. J. C* **78**, 1 (2018)
- [81] B. Patel and P. C. Vinodkumar, *J. Phys. G: Nucl. Part. Phys.* **36**, 035003 (2009)
- [82] A. M. Badalian, B. L. G. Bakker, and I. V. Danilkin, *Phys. Rev. D* **79**, 037505 (2009)
- [83] J. Segovia, P. G. Ortega, D. R. Entem, and F. Fernandez, *Phys. Rev. D* **93**, 074027 (2016)
- [84] A. K. Grant and J. L. Rosner, *Phys. Rev. D* **46**, 3862 (1992)
- [85] E. Eichten, S. Godfrey, H. Mahlke, and J. L. Rosner, *Rev. Mod. Phys.* **80**, 1161 (2008)
- [86] A. M. Badalian and B. L. G. Bakker, *Phys. Rev. D* **86**, 074001 (2012)
- [87] A. Abdesselam, I. Adachi, K. Adamczyk, H. Aihara, S. A. Said, *et al.*, arXiv 10.48550/arXiv.1606.01276 (2016), 1606.01276.
- [88] C. Cawlfeld, B. I. Eisenstein, I. Karliner, D. Kim, N. Lowrey, *et al.*, *Phys. Rev. D* **73**, 012003 (2006)